



저작자표시-비영리-변경금지 2.0 대한민국

이용자는 아래의 조건을 따르는 경우에 한하여 자유롭게

- 이 저작물을 복제, 배포, 전송, 전시, 공연 및 방송할 수 있습니다.

다음과 같은 조건을 따라야 합니다:



저작자표시. 귀하는 원저작자를 표시하여야 합니다.



비영리. 귀하는 이 저작물을 영리 목적으로 이용할 수 없습니다.



변경금지. 귀하는 이 저작물을 개작, 변형 또는 가공할 수 없습니다.

- 귀하는, 이 저작물의 재이용이나 배포의 경우, 이 저작물에 적용된 이용허락조건을 명확하게 나타내어야 합니다.
- 저작권자로부터 별도의 허가를 받으면 이러한 조건들은 적용되지 않습니다.

저작권법에 따른 이용자의 권리는 위의 내용에 의하여 영향을 받지 않습니다.

이것은 [이용허락규약\(Legal Code\)](#)을 이해하기 쉽게 요약한 것입니다.

[Disclaimer](#)

공학박사학위논문

나노초 펄스 레이저를 이용한  
실리콘 화합물 세라믹의  
수열 반응 레이저 빔 가공

Hydrothermal Reactive Laser Beam Machining for  
Silicon Compound Ceramics using Nanosecond Pulsed Laser

2020 년 2 월

서울대학교 대학원

기계항공공학부

정 형 균

**HYDROTHERMAL REACTIVE  
LASER BEAM MACHINING FOR  
SILICON COMPOUND CERAMICS  
USING NANOSECOND PULSED LASER**

**DISSERTATION**

SUBMITTED TO THE SCHOOL OF MECHANICAL AND  
AEROSPACE ENGINEERING AND THE COMMITTEE ON  
GRADUATE STUDIES OF SEOUL NATIONAL UNIVERSITY  
IN PARTIAL FULFILLMENT OF THE REQUIREMENTS  
FOR THE DEGREE OF DOCTOR OF PHILOSOPHY

Hyeong Gyun Cheong

February 2020

# Abstract

Hyeong-Gyun Cheong

Department of Mechanical and Aerospace Engineering

The Graduate School

Seoul National University

In this dissertation, hydrothermal reactive laser beam machining of silicon compound ceramics was investigated. Silicon compound ceramics have been widely used in engineering applications due to their outstanding properties such as high-temperature strength, wear resistance, and chemical resistance. However, their superior properties have made the materials hard to micro-machine, limiting the efficient use of the materials in industry. In the machining of silicon compound ceramic materials via laser beam, processing in water has been found to enhance machining quality, while processing in air has limitations such as the generation of a recast layer, heat affected zone, and thermal crack. However, few studies have investigated the effects of water on the ablation rate of silicon compound ceramics.

In this research, the ablation behavior and machining principles of the laser beam machining of silicon compound ceramics in water are investigated. The research concluded that the increase in temperature induced by laser irradiation promotes hydrothermal reaction between the silicon compound ceramics and water. The hydrothermal reaction assists in the removal of the oxide layer at the machined area and enhances the efficiency of the process in water. The effects of water on ablation are confirmed for various machining parameters such as the flow rate of sprayed water on the workpiece and laser conditions. As the flow rate of water increased, a deeper and narrower groove was able to be machined. Also, compared to grooves machined in air, the deeper groove was able to be machined in water under the same machining conditions. Finally, the various micro-structures such as micro-channel arrays, micro-pin arrays and micro-slit were fabricated on the silicon compound ceramics to evaluate the processability. By using hydrothermal reactive laser beam machining, machining efficiency in micro-structuring of silicon compound ceramics can be improved with high machining quality.

**Keyword:** Underwater laser beam machining; Silicon compound ceramics; Silicon nitride; Silicon carbide; Hydrothermal reaction; Micro-structuring

**Student Number:** 2014-21837

# Contents

<b>Abstract</b> .....	i
<b>Contents</b> .....	iii
<b>List of Figures</b> .....	vi
<b>List of Tables</b> .....	xiii
<b>Chapter 1. Introduction</b> .....	- 1 -
1.1. Research background .....	- 1 -
1.2. Research objective .....	- 10 -
1.3. Dissertation overview .....	- 11 -
<b>Chapter 2. Hydrothermal reactive laser beam machining of silicon compound ceramics</b> .....	- 13 -
2.1. Underwater laser beam machining.....	- 13 -
2.2. Hydrothermal corrosion of silicon compound ceramics .....	- 15 -
2.3. Experimental setup and procedures .....	- 17 -

2.4. Laser beam energy under a thin water film .....	- 20 -
<b>Chapter 3. Machining mechanism investigation .....</b>	<b>- 23 -</b>
3.1. Ablation behavior in air and water.....	- 23 -
3.2. Effect of hydrothermal reaction during underwater LBM.....	- 33 -
<b>Chapter 4. Machining characteristics.....</b>	<b>- 45 -</b>
4.1. Effect of flow rates of water .....	- 46 -
4.2. Effect of laser conditions .....	- 49 -
4.2.1. Laser power .....	- 49 -
4.2.2. Scan repeat count .....	- 56 -
4.2.3. Scan speed .....	- 60 -
<b>Chapter 5. Fabrication of various micro structure .....</b>	<b>- 65 -</b>
5.1. Micro channel .....	- 66 -
5.2. Micro pin.....	- 73 -
5.3. Cutting .....	- 82 -

<b>Chapter 6. Conclusion</b> .....	- 87 -
<b>Reference</b> .....	- 90 -
<b>국문 초록</b> .....	- 100 -



# List of Figures

- Figure 1.1 Comparison of machining characteristics in previous micro structuring process for silicon compound ceramics and underwater laser beam machining
- Figure 2.1 Schematic presentation of hydrothermal corrosion of  $\text{Si}_3\text{N}_4$  and  $\text{SiC}$ : (a) oxidation of silicon nitride and silicon carbide in water ( $< 200^\circ\text{C}$ ), (b) dissolution of amorphous silica in water ( $>200^\circ\text{C}$ )
- Figure 2.2 Schematic diagram of experimental setup for the laser beam machining under a thin water film
- Figure 2.3 Refractions of a laser beam through water media
- Figure 3.1 SEM micrographs of cavities in silicon compound ceramics machined by the laser beam: (a, c) in air, (b, d) in water
- Figure 3.2 Cross section views of cavities machined by the laser beam on the  $\text{Si}_3\text{N}_4$  surface according to scan repeat count (3 W of laser power, 100 mm/s of scan speed): (a, b, c, d) in air, (e, f, g, h) in water
- Figure 3.3 Cross section views of cavities machined by the laser beam on the  $\text{SiC}$  surface according to scan repeat count (8 W of laser power, 100 mm/s of scan speed): (a, b, c, d) in air, (e, f, g, h) in water

- Figure 3.4 SEM micrographs of  $\text{Si}_3\text{N}_4$  surfaces in different laser ablation conditions: (a) reference  $\text{Si}_3\text{N}_4$  surface; (b) laser ablation in air; (c) laser ablation in water
- Figure 3.5 SEM micrographs of  $\text{SiC}$  surfaces in different laser ablation conditions: (a) reference  $\text{SiC}$  surface; (b) laser ablation in air; (c) laser ablation in water
- Figure 3.6 EDS map analysis of oxygen on the cross section surfaces ablated by the laser in air: (a)  $\text{Si}_3\text{N}_4$ , (b)  $\text{SiC}$
- Figure 3.7 EDS map analysis of silicon on the cross section surfaces ablated by the laser in air: (a)  $\text{Si}_3\text{N}_4$ , (b)  $\text{SiC}$
- Figure 3.8 XPS spectra for surfaces of  $\text{Si}_3\text{N}_4$  and  $\text{SiC}$  machined by the laser beam in air: (a) O 1s, (b) Si 2p
- Figure 3.9 Reaction diagram for the hydrothermal reaction of silicon compound ceramics
- Figure 3.10 Reaction diagram for the hydrothermal reaction of silicon compound ceramics
- Figure 3.11 Schematic diagram of the experiments to investigate the chemical effects of water on the removal of  $\text{SiO}_2$
- Figure 3.12 SEM micrographs of  $\text{Si}_3\text{N}_4$  surfaces in different laser ablation conditions: (a) laser ablation in air; (b) laser irradiation in water after laser ablation in air; (c) laser irradiation in kerosene after laser ablation in air

- Figure 3.13 SEM micrographs of SiC surfaces in different laser ablation conditions: (a) laser ablation in air; (b) laser irradiation in water after laser ablation in air; (c) laser irradiation in kerosene after laser ablation in air
- Figure 3.14 Schematic diagram for material removal mechanism during LBM of silicon compound ceramics in air and water
- Figure 4.1 The relation between dimensions of channel and flow rate of water when machining silicon compound ceramics by laser beam in water: (a) Si<sub>3</sub>N<sub>4</sub>, (b) SiC
- Figure 4.2 Cross section views of micro-channels in Si<sub>3</sub>N<sub>4</sub> obtained by laser beam machining in water with different flow rate of water: (a) 2 ml/s; (b) 3 ml/s; (c) 4 ml/s; (d) 5 ml/s
- Figure 4.3 Cross section views of micro-channels in SiC obtained by laser beam machining in water with different flow rate of water: (a) 2 ml/s; (b) 3 ml/s; (c) 4 ml/s; (d) 5 ml/s
- Figure 4.4 Tendency of depth and width of grooves machined in air and water on the Si<sub>3</sub>N<sub>4</sub> surfaces according to laser power
- Figure 4.5 Tendency of depth and width of grooves machined in air and water on the SiC surfaces according to laser power
- Figure 4.6 Cross section views of micro-channels in Si<sub>3</sub>N<sub>4</sub> obtained by laser beam machining with different laser power: (a) in water, (b) in air
- Figure 4.7 Cross section views of micro-channels in SiC obtained by laser beam machining with different laser power: (a) in water, (b) in air

- Figure 4.8 Laser intensity graph with a Gaussian distribution
- Figure 4.9 Principle of width expansion with increasing laser power
- Figure 4.10 Tendency of depth and width of grooves machined in air and water on the  $\text{Si}_3\text{N}_4$  surfaces according to scan repeat count
- Figure 4.11 Tendency of depth and width of grooves machined in air and water on the  $\text{SiC}$  surfaces according to scan repeat count
- Figure 4.12 Cross section views of micro-channels in  $\text{Si}_3\text{N}_4$  obtained by laser beam machining with different scan repeat count: (a) in water, (b) in air
- Figure 4.13 Cross section views of micro-channels in  $\text{Si}_3\text{N}_4$  obtained by laser beam machining with different scan repeat count: (a) in water, (b) in air
- Figure 4.14 The relation between dimensions of channel and flow rate of water when machining silicon compound ceramics by laser beam in water: (a)  $\text{Si}_3\text{N}_4$ , (b)  $\text{SiC}$
- Figure 4.15 Cross section views of micro-channels obtained by hydrothermal reactive laser beam machining with different scan speed: (a)  $\text{Si}_3\text{N}_4$ , (b)  $\text{SiC}$
- Figure 5.1 Multiple scan paths used in micro-channel machining
- Figure 5.2 The relation between dimensions of channel and line interval when machining silicon compound ceramics by laser beam in water: (a)  $\text{Si}_3\text{N}_4$ , (b)  $\text{SiC}$

- Figure 5.3 Cross section views of micro-channels in  $\text{Si}_3\text{N}_4$  obtained by laser beam machining in water with different line interval: (a) 10  $\mu\text{m}$ ; (b) 20  $\mu\text{m}$ ; (c) 30  $\mu\text{m}$ ; (d) 40  $\mu\text{m}$ ; (e) 50  $\mu\text{m}$ ; (f) 60  $\mu\text{m}$ ; (g) 70  $\mu\text{m}$ ; (h) 80  $\mu\text{m}$
- Figure 5.4 Cross section views of micro-channels in  $\text{SiC}$  obtained by laser beam machining in water with different line interval: (a) 10  $\mu\text{m}$ ; (b) 20  $\mu\text{m}$ ; (c) 30  $\mu\text{m}$ ; (d) 40  $\mu\text{m}$ ; (e) 50  $\mu\text{m}$ ; (f) 60  $\mu\text{m}$ ; (g) 70  $\mu\text{m}$ ; (h) 80  $\mu\text{m}$
- Figure 5.5 SEM micrographs of micro-channel arrays using hydrothermal reactive laser beam machining using multiple scan path: (a-d) in  $\text{Si}_3\text{N}_4$ , (e-h) in  $\text{SiC}$
- Figure 5.6 SEM micrographs of wedged micro-channel arrays using hydrothermal reactive laser beam machining: (a, b) in  $\text{Si}_3\text{N}_4$ , (c, d) in  $\text{SiC}$
- Figure 5.7 SEM micrographs of waved micro-channel arrays using hydrothermal reactive laser beam machining: (a, b) in  $\text{Si}_3\text{N}_4$ , (c, d) in  $\text{SiC}$
- Figure 5.8 SEM micrographs of micro-pin arrays machined in  $\text{Si}_3\text{N}_4$ : (a) using a single laser scan path by LBM in water; (b) using a single laser scan path by LBM in air; (c) using multiple scan paths by LBM in air
- Figure 5.9 Laser scan path used to fabricate micro-pin arrays: (a) a single laser scan path, (b) multiple laser scan path

- Figure 5.10 Cross section views and tilted views of micro-pin arrays in  $\text{Si}_3\text{N}_4$  obtained by hydrothermal reactive laser beam machining with different line space: (a) 80  $\mu\text{m}$ ; (b) 90  $\mu\text{m}$ ; (c) 100  $\mu\text{m}$ ; (d) 110  $\mu\text{m}$
- Figure 5.11 Cross section views and tilted views of micro-pin arrays in  $\text{SiC}$  obtained by hydrothermal reactive laser beam machining with different line space: (a) 80  $\mu\text{m}$ ; (b) 90  $\mu\text{m}$ ; (c) 100  $\mu\text{m}$ ; (d) 110  $\mu\text{m}$
- Figure 5.12 Cross section views and tilted views of micro-pin arrays in  $\text{Si}_3\text{N}_4$  obtained by hydrothermal reactive laser beam machining with different scan repeat count: (a) 1000 times; (b) 3000 times; (c) 5000 times; (d) 7000 times
- Figure 5.13 Cross section views and tilted views of micro-pin arrays in  $\text{SiC}$  obtained by hydrothermal reactive laser beam machining with different scan repeat count: (a) 1000 times; (b) 2000 times; (c) 3000 times; (d) 4000 times
- Figure 5.14 Tilted views of micro-pin arrays in  $\text{Si}_3\text{N}_4$  obtained by laser beam machining with different line space: (a) 40  $\mu\text{m}$ ; (b) 50  $\mu\text{m}$ ; (c) 60  $\mu\text{m}$ ; (d) 70  $\mu\text{m}$
- Figure 5.15 Tilted views of micro-pin arrays in  $\text{Si}_3\text{N}_4$  obtained by laser beam machining with different repeat count: (a) 1 times; (b) 10 times; (c) 50 times; (d) 100 times
- Figure 5.16 Tilted views of micro-pin arrays in  $\text{SiC}$  obtained by hydrothermal reactive laser beam machining with different line space: (a) 40  $\mu\text{m}$ ; (b) 50  $\mu\text{m}$ ; (c) 60  $\mu\text{m}$ ; (d) 70  $\mu\text{m}$

- Figure 5.17 Tilted views of micro-pin arrays in SiC obtained by laser beam machining with different repeat count: (a) 1 times; (b) 10 times; (c) 30 times; (d) 50 times
- Figure 5.18 Comparison of the micro-pin array fabricated by laser beam machining in air and water
- Figure 5.19 Cross section views and tilted views of Si<sub>3</sub>N<sub>4</sub> sheet cut by hydrothermal reactive laser beam machining: (a, b) thickness of 0.5 mm; (c, d) thickness of 1 mm
- Figure 5.20 Cross section views and tilted views of SiC sheet cut by hydrothermal reactive laser beam machining: (a, b) thickness of 0.5 mm; (c, d) thickness of 1 mm
- Figure 5.21 SEM micrographs of silicon compound ceramics sheets cut by hydrothermal reactive laser beam machining using various scan path: (a-d) in Si<sub>3</sub>N<sub>4</sub>, (e-h) in SiC

# List of Tables

Table 1.1	Applications of different engineering ceramics
Table 1.2	The characteristics of various machining process to texture micro structure on ceramic surface
Table 3.1	EDS results for elemental compositions of Si <sub>3</sub> N <sub>4</sub> before and after laser ablation
Table 3.2	EDS results for elemental compositions of SiC before and after laser ablation
Table 3.3	Thermodynamic properties and measured absorbance values of Si <sub>3</sub> N <sub>4</sub> , SiC, and SiO <sub>2</sub>
Table 3.4	Standard thermodynamic values of the elements in hydrothermal reaction at 25°C
Table 3.5	EDS results for elemental compositions of Si <sub>3</sub> N <sub>4</sub> before and after laser ablation
Table 3.6	EDS results for elemental compositions of SiC before and after laser ablation
Table 4.1	Summary of the effects of laser conditions on the grooves machined in air and water
Table 5.1	Machining conditions and resulted dimension in cutting of Si <sub>3</sub> N <sub>4</sub> and SiC sheets with a thickness of 0.5 mm and 1 mm
Table 5.2	Comparison of hydrothermal reactive LBM of silicon compound ceramics with other processes



# Chapter 1

## Introduction

### 1.1. Research Background

Silicon compound ceramics such as silicon nitride ( $\text{Si}_3\text{N}_4$ ) and silicon carbide ( $\text{SiC}$ ) have been widely used in engineering applications due to their outstanding properties such as high-temperature strength, wear resistance, and chemical resistance [1]. In particular,  $\text{Si}_3\text{N}_4$  and  $\text{SiC}$  have been the primary solutions in several micro-engineering applications such as wear parts, cutting tools, heat engine components, etc. Because of higher thermal shock resistance and plasma durability than other conventional ceramics, silicon compound ceramics also has been used for components of semiconductor manufacturing equipment. Especially, components for semiconductor manufacturing equipment needs precise tolerance, precision machining of silicon compound ceramics has been necessary. In addition, as use of silicon compound ceramics has been increased, the importance of

surface texturing and surface structuring of silicon compound ceramics have been increased. By surface texturing and structuring, many functionality such as high thermal efficiency, wettability control, and friction reduction can be applied on silicon compound ceramic surface. For example, by surface texturing, the friction coefficient and wear resistance can be improved. Since silicon compound ceramics has been used for wear parts such as mechanical seals, and high speed bearing, the surface structuring of silicon compound ceramics can contribute to the improvement of performance in silicon compound ceramics wear parts. Table 1.1 shows applications of different engineering ceramics including  $\text{Si}_3\text{N}_4$  and  $\text{SiC}$ .

However, their superior properties have made the materials hard to micro-machine, limiting the efficient use of the materials in industry. Conventional machining, including micro-grinding, abrasive waterjet machining, and ultrasonic machining, has its own limitations such as surface crack, high residual stress, and tool wear in the micro-machining of the materials [2–6]. Abrasive waterjet machining is one of mechanical machining process used to cut brittle materials. However, coarse cutting surface, wide channel width and crack generation limits use of abrasive machining in micro-structuring. In addition, abrasive waterjet machining is difficult to machine silicon compound ceramics due to high mechanical strength compared with other

engineering ceramics. Micro EDM is one of noncontact machining method which can machine ceramics with high accuracy without mechanical defect [7–9]. However, to use micro EDM, doping of conductive material in ceramics or attaching of assisted electrode on ceramics surface must be needed, because EDM can machine only conductive material [10–12]. Also tool wear and low machining speed are disadvantage of the process.

**Table 1.1 Applications of different engineering ceramics [1].**

Application	Performance advantages	Examples
Wear parts: seals, bearings, valves, nozzles	High hardness, low friction	SiC, Al <sub>2</sub> O <sub>3</sub>
Cutting tools	High strength, hardness	Si <sub>3</sub> N <sub>4</sub>
Heat engines: diesel components, gas turbines	Thermal insulation, high-temperature strength, fuel economy	ZrO <sub>2</sub> , SiC, Si <sub>3</sub> N <sub>4</sub>
Medical implants: hips, teeth, joints	Biocompatibility, surface bond to tissue, corrosion resistance	Bioglass, Al <sub>2</sub> O <sub>3</sub> , ZrO <sub>2</sub>
Construction: highways, bridges, buildings	Improved durability, lower overall cost	Advanced cements and concrete

Laser beam machining (LBM) is a noncontact machining process that has been an effective method for machining ceramics [13–16]. Because laser beam machining ablates materials without mechanical stress on the workpiece, it can machine hard-to-cut materials regardless of hardness. LBM also has several advantages such as high resolution, high processing speed, and no tool requirement. As a result, LBM of silicon compound ceramics have been studied by many researchers [17–20]. Due to the thermal effect, several defects were noted such as thermal residual stress, thermal crack, change in chemical composition, and the generation of a recast layer. The femtosecond laser can significantly reduce the thermal residual stress and thermal crack of the materials [21]. However, the low productivity, costly investment, and difficulties in treating the system make the widespread use of the femtosecond laser difficult in industry.

To solve the problems of LBM of ceramics, LBM in water media has been investigated. The research of LBM in water has been performed on various materials, including silicon compound ceramics, and the effects of water on machining quality have been confirmed [22,23]. LBM in water has been found to reduce recast layer, heat affected zone, and surface crack. Morita [24] showed that the recast layer and micro cracks were removed from  $\text{Si}_3\text{N}_4$  by LBM in water. They concluded water solidified and removed molten debris

through the flushing of water. Dolgaev [25] demonstrated that an oxide layer was not formed with LBM in water, while LBM in air generated an oxide layer on the SiC surface. They concluded the oxide layer was removed by the dynamic impact of the expanding water layer. Geiger [26] compared the ablation rates of various engineering ceramics including Si<sub>3</sub>N<sub>4</sub> and SiC for LBM in air and water. They used an excimer laser and revealed the ablation rates of Si<sub>3</sub>N<sub>4</sub> and SiC decreased through the use of water during LBM; this could not be adequately explained. Micro drilling at 330 μm-thick SiC by LBM in water was conducted by Wee [27] and the micro-structuring of various ceramics including Si<sub>3</sub>N<sub>4</sub> and SiC using LBM in water was carried out by Geiger [28]. These studies demonstrate that the water layer improves the quality of microstructures during LBM of silicon compound ceramics. Table 1.2 shows the characteristics of various machining process to texture micro structure on ceramic surface.

**Table 1.2 The characteristics of various machining process to texture micro structure on ceramic surface.**

Process	Characteristics	Limitation
Micro cutting /grinding	<ul style="list-style-type: none"> <li>● Traditional contact machining</li> <li>● High machining speed</li> </ul>	<ul style="list-style-type: none"> <li>● Tool breakage</li> <li>● High tool wear</li> <li>● Surface cracks</li> </ul>
Abrasive waterjet machining	<ul style="list-style-type: none"> <li>● Erosive wear by a blast of abrasive-laden water stream</li> </ul>	<ul style="list-style-type: none"> <li>● Low straightness</li> <li>● Taper</li> <li>● Residual stress</li> </ul>
Ultrasonic machining	<ul style="list-style-type: none"> <li>● Removing ceramics by vibration of micro tool at high speed</li> </ul>	<ul style="list-style-type: none"> <li>● Surface cracks</li> <li>● Spalling</li> <li>● Low machining speed</li> </ul>
EDM	<ul style="list-style-type: none"> <li>● High Accuracy</li> <li>● Noncontact machining</li> <li>● Need of conductivity</li> </ul>	<ul style="list-style-type: none"> <li>● Need of doping conductive material</li> <li>● Need of attaching assisted electrode</li> <li>● Tool wear</li> <li>● Low speed</li> </ul>
Sintering	<ul style="list-style-type: none"> <li>● Traditional process</li> <li>● High productivity</li> <li>● Binding process under high temperature and pressure</li> </ul>	<ul style="list-style-type: none"> <li>● Low precision (shrinkage)</li> <li>● Cost consuming (Mold, temperature and pressure controller)</li> </ul>

LBM (Nanosecond)	<ul style="list-style-type: none"> <li>● Non-contact machining</li> <li>● No tool requirement</li> <li>● High machining speed</li> </ul>	<ul style="list-style-type: none"> <li>● Low accuracy</li> <li>● Recast layer</li> <li>● Chemical composition change</li> <li>● Thermal crack</li> </ul>
LBM (Femtosecond)	<ul style="list-style-type: none"> <li>● High accuracy</li> <li>● Low thermal residual stress and crack</li> </ul>	<ul style="list-style-type: none"> <li>● Low productivity</li> <li>● Costly investment</li> <li>● Difficulties in treating the system</li> </ul>
Underwater LBM	<ul style="list-style-type: none"> <li>● Improved machining quality</li> <li>● Reduced re-deposition of recast layer</li> <li>● Reduced thermal crack</li> </ul>	<ul style="list-style-type: none"> <li>● Decreased machining efficiency</li> <li>● Laser beam scattering by bubbles and debris</li> <li>● Energy absorption of water and debris</li> </ul>

Although the effects of water on the quality of machined surfaces have been found in silicon compound ceramics in previous research, the efficiency of the process varied in each case depending on laser conditions and the water supply system. The effects of water on the ablation rate were not sufficiently presented and there was a lack of clear explanation for the difference in ablation rates between when water was used or not. Also, the machining mechanism and chemical reaction inherent in silicon compound ceramics

were deficient. Therefore, it is still worthwhile to study the LBM of silicon compound ceramics in water to determine the mechanism of material removal and clearly analyze the machining characteristics of each parameter. Figure 1.1 shows one example of limitation of previous micro structuring technology for silicon compound ceramics. Although versatile machining technologies for silicon compound ceramic has been used over a wide range, each process has limitation in machining quality and efficiency. These issues clearly contributed to the development of the micro structuring technologies of silicon compound ceramics.



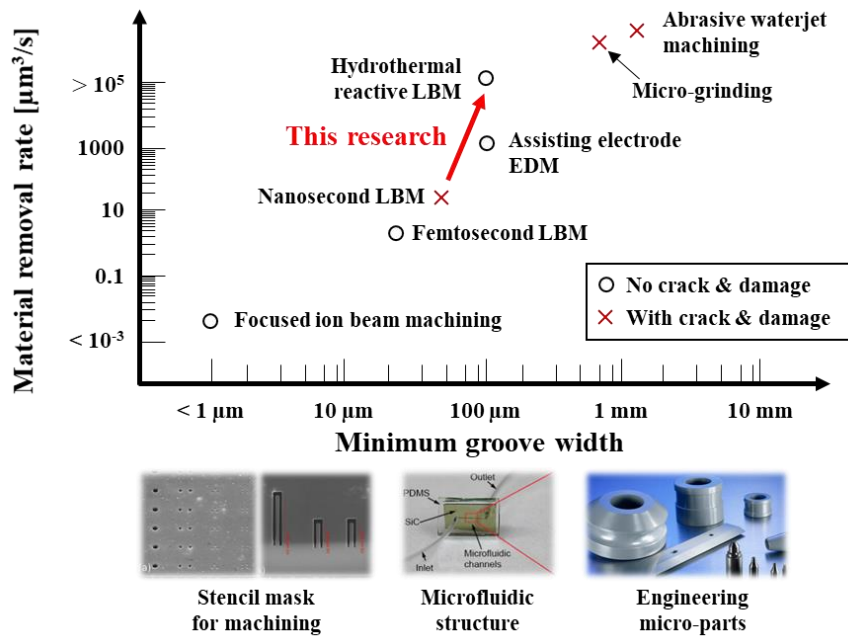


**Fig. 1.1 Comparison of machining characteristics in previous micro structuring process for silicon compound ceramics and underwater laser beam machining.**

## **1.2. Research Objective**

In this research, the ablation behavior and machining principle were investigated during the structuring of silicon compound ceramics using LBM in water. The nanosecond pulsed laser widely utilized in industry applications was used for the experiment. The ablation behaviors in air and water were observed during micro-cavity machining. To determine the machining principle for LBM of silicon compound ceramics in water, the laser beam was irradiated in water and kerosene and the chemical compositions of the machined surface were measured by energy-dispersive X-ray spectroscopy. Also, the effects of machining parameters such as the flow rate of water, laser power, and scan repeat rate during groove machining were investigated. Finally, arrays of micro-channels were fabricated on the silicon compound ceramics to demonstrate various structuring is possible using LBM in water.

### **1.3. Dissertation Overview**

In chapter 1, the main issues for dealing with previous processes for structuring on ceramics material were introduced. The importance of the micro machining of silicon compound ceramics and limits of various previous processes to micro-machine silicon compound ceramics were presented. In this chapter, research background, the necessity of the research for hydrothermal reactive LBM of silicon compound ceramics, and research objective were introduced.

In chapter 2, background theory of the hydrothermal reactive LBM was presented. Also, background theory of relevant subject with hydrothermal reactive LBM of silicon compound ceramics were explained such as laser beam energy calculation during underwater LBM and hydrothermal reaction of the silicon compound ceramics were explained. Experimental setup and procedures were presented in this chapter.

In chapter 3, machining mechanism in hydrothermal reactive LBM of silicon compound ceramics was investigated. Ablation behavior of silicon compound ceramics in air and water were observed, and chemical composition analysis of the ablated area was conducted. The effect of

hydrothermal reaction on the underwater laser beam machining of silicon compound ceramics was verified by chemical composition analysis and oxide removal experiments in water and kerosene.

In chapter 4, machining characteristics in hydrothermal reactive LBM of silicon compound ceramics were investigated. Parametric study for flow rates of water and laser conditions such as laser power, scan repeat count, and scan speed were conducted. Proper machining conditions for micro structuring of silicon compound ceramics were suggested additionally.

In chapter 5, various micro structures were fabricated on silicon compound ceramics using hydrothermal reactive LBM to evaluate processability. Micro-channel arrays and micro-pin arrays were fabricated and micro-cutting was conducted. As changing the laser scan path, various shape structure were able to be fabricated.

In chapter 6, conclusion and discussion of this dissertation were presented.

# **Chapter 2**

## **Hydrothermal reactive Laser Beam Machining of Silicon Compound Ceramics**

### **2.1. Underwater Laser Beam Machining**

Underwater laser beam machining (underwater LBM) is laser beam machining process which ablates materials under water. Underwater LBM can machine material with better tolerances and reduce negative thermal effects such as thermal residual stress, thermal crack, chemical composition change, and heat affected zone. Generally, underwater LBM has been used to increase machining quality by elimination of debris redeposition in the machined surface [1]. The thermal convection of water and liquid motion induced by bubble carry the debris during the underwater LBM. By using underwater LBM, after-cleaning process such as ultrasonic vibration in solution can be skipped. Also, underwater LBM can be used for machining heat-sensitive materials, such as HgCdTe to avoid decomposition of workpiece during the LBM process [29]. Ceramics can be machined by underwater LBM to avoid thermal crack during the LBM process [24]. Underwater LBM has

advantage in machining diamond, because it is effective to remove graphitized layer which decreases the catalytic activity of diamond for metal deposition [30]. Likewise, underwater LBM can be used for machining SiC to avoid silicon layer formation which leads to catalytic activity of metal deposition [25,31].

Until now, underwater LBM of various materials has been researched including metals, alloys, ceramics, glass, and polymers [28–30,32–38]. However, the differences of ablation rate between LBM in air and in water were varied depending on the materials. Some materials showed lower ablation rate in water than in air, for example different metals, stainless steel, ZrO<sub>2</sub>, SiC, Si<sub>3</sub>N<sub>4</sub>, polyamide, and NdFeB [26,28,35]. Other materials showed higher ablation rate in water than in air, for example Al, Si, SiO<sub>2</sub>, and Al<sub>2</sub>O<sub>3</sub> [34,36,39]. There are some possible reasons for the reason that laser ablation rate differs in water. Bubbles and debris in water reduce transparency of water and it can lead to decrease of ablation rate in water [25]. On the other hand, the possible reasons for the increase in ablation rate in water is as follows: high temperature of confined plasma [39], microjets induced by shock wave [25,26], flushing by liquid motion [34]. Nevertheless, there are no satisfactory explanations for such material behavior. Also, researches to improve ablation rate decreased during underwater LBM were deficient. Therefore, it is still worthwhile to study the LBM of silicon compound ceramics in water to determine the mechanism of material removal and improve machining efficiency during the underwater LBM of silicon compound ceramics.

## 2.2. Hydrothermal Corrosion of Silicon Compound Ceramics

The corrosion behavior of silicon compound ceramics including silicon nitride ( $\text{Si}_3\text{N}_4$ ) and silicon carbide ( $\text{SiC}$ ) at high temperatures has been reported by several researchers [40–44]. Under hydrothermal conditions, the silicon compound ceramics corrode noticeably, which leads to the degradation of fracture strength and significant weight loss. The corrosion reaction under hydrothermal conditions is as follows:

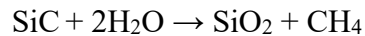
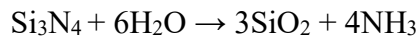
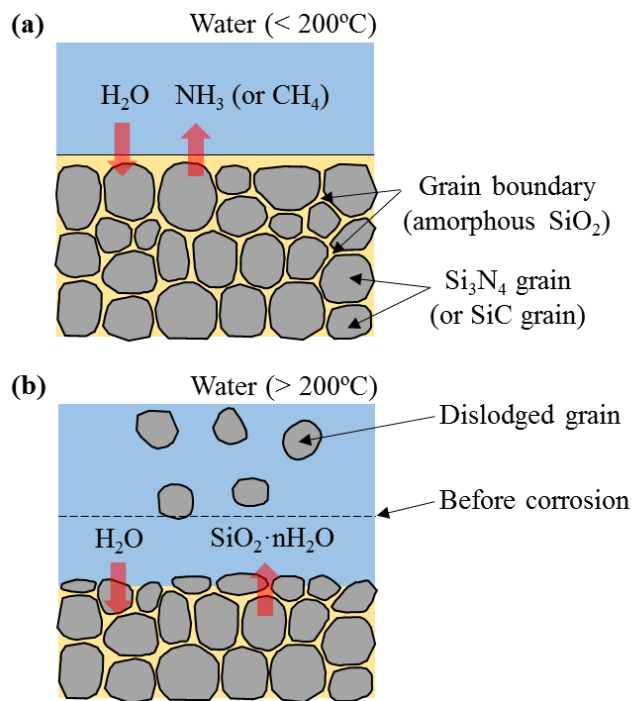


Figure 2.3 shows a schematic representation of the corrosion procedure of  $\text{Si}_3\text{N}_4$  and  $\text{SiC}$  in hydrothermal conditions. In high temperature water, the oxidation reaction rate of the materials is accelerated by the increasing temperature (Fig. 2.3 a). At room temperature, the stable silica layer protects the materials in aqueous solutions. The solubility of silica, however, greatly increases with increasing temperatures over  $200^\circ\text{C}$ – $250^\circ\text{C}$  (Fig. 2.3 b). A series of dissolution reaction of silica in water is as follow [45]:



Therefore, the  $\text{Si}_3\text{N}_4$  and  $\text{SiC}$  showed significant dissolution rates in water over the temperature range of  $200^\circ\text{C} - 250^\circ\text{C}$ .



**Fig. 2.3 Schematic presentation of hydrothermal corrosion of silicon nitride and silicon carbide: (a) oxidation of silicon nitride and silicon carbide in water ( $< 200^\circ\text{C}$ ), (b) dissolution of amorphous silica in water ( $> 200^\circ\text{C}$ ).**



## **2.3. Experimental Setup and Procedures**

The experimental system is depicted in Figure 2.1. An ytterbium-doped fiber laser (YLP-C-1-100-20-20, IPG, Germany) with a wavelength of 1,064 nm, pulse duration of 100 ns, and spot diameter of 42  $\mu\text{m}$  was used in the experiments. The laser beam was irradiated through a galvanometer scanner (SCANcube® 10, Scanlab, Germany) with a specified scanning speed. The scanner was installed on the Z-stage to adjust the focal point on a workpiece and the X- and Y-stages were used to control the position of the workpiece. The stages were controlled in 0.1  $\mu\text{m}$  resolution using a motion controller. A DC pump with a flow rate controller was used for spraying water on the workpiece when the laser beam machining was processing in water.

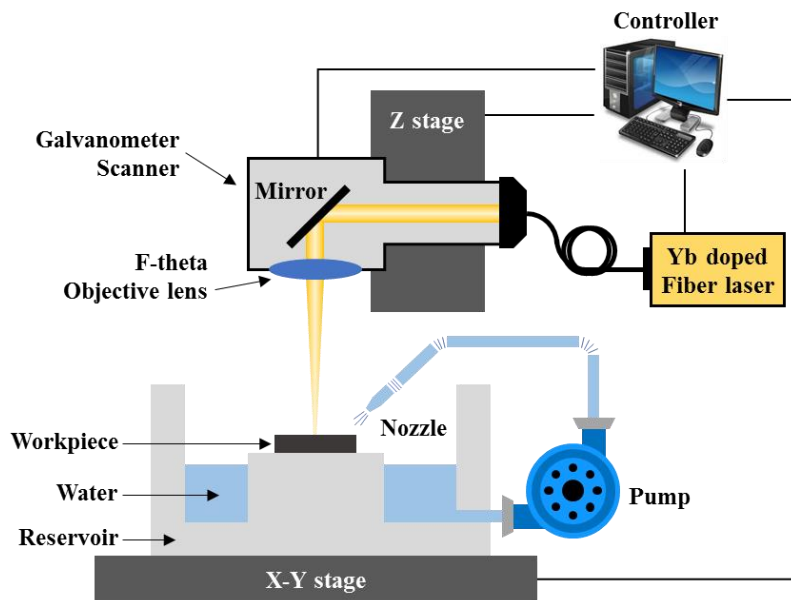


**Fig. 2.1 Schematic diagram of experimental setup for the laser beam machining under a thin water film.**

The workpiece materials and machining conditions are described in Table 1. Silicon nitride ( $\text{Si}_3\text{N}_4$ , Nagamine Manufacturing Co. Ltd., Japan) and silicon carbide ( $\text{SiC}$ , Nagamine Manufacturing Co. Ltd., Japan) were used in the experiments as silicon compound ceramic workpieces. Water was sprayed onto the surface of the workpiece to submerge the workpiece under water and played a role in removing debris and bubbles at the machined area. By controlling the flow rate above 2 ml/s, the thickness of water on the workpiece was maintained at less than 500  $\mu\text{m}$  during the machining process. For  $\text{Si}_3\text{N}_4$  and  $\text{SiC}$ , a laser power of 6 W and 8 W were set as the basic process conditions. In the same manner, a 100 mm/s scan speed and 5 ml/s flow rate were set as the basic process conditions for both materials. A cross section of structures machined by laser were observed using a scanning electron microscope (SEM) (JSM-6360, JEOL, Japan). To observe the chemical composition changes in the laser processed area, energy-dispersive X-ray spectroscopy (EDS) (MERLIN Compact, Zeiss, Germany) and X-ray photoelectron spectroscopy (XPS) (AXIS-His, KRATOS, Japan) were performed.

## 2.4. Laser Beam Energy under a Thin Water Film

When a laser beam passes through water, the intensity of the laser beam at the workpiece surface is reduced due to the light absorption of water even when the light absorption of debris and light scattering of bubbles are not assumed. Also, the focal distance is shifted from the initial point due to the refraction of the laser beam in water. These factors need to be calculated as they influence material ablation. According to Beer-Lambert's law, the laser intensity after traveling in water ( $I$ ) is determined as follows:

$$I = I_0 \exp(-\alpha h)$$

$I_0$ ,  $\alpha$ , and  $h$  are the initial laser intensity, the absorption coefficient of water (0.00168/cm for a wavelength of 1,064 nm) [46], and the thickness of the water, respectively. The refraction of the laser in water is shown in Figure 2. According to Snell's law, the refracted angle of the laser beam in water ( $\theta_w$ ) can be calculated. Also, the focal distance shifted from the initial position ( $Z_s$ ) can be deduced by geometrical calculation of the refracted angle as follows:

$$\theta_w = \sin^{-1} \left\{ \frac{n_a}{n_w} \sin \left( \tan^{-1} \frac{D}{2F} \right) \right\}$$

$$Z_s = h \left\{ 1 - 2F \frac{\tan \theta_w}{D} \right\}$$

$n_a$ ,  $n_w$ ,  $D$ , and  $F$  are the refractive index of air (1.0), refractive index of water (1.333), collimated laser beam diameter (7.6 mm), and focal length (160 mm), respectively.

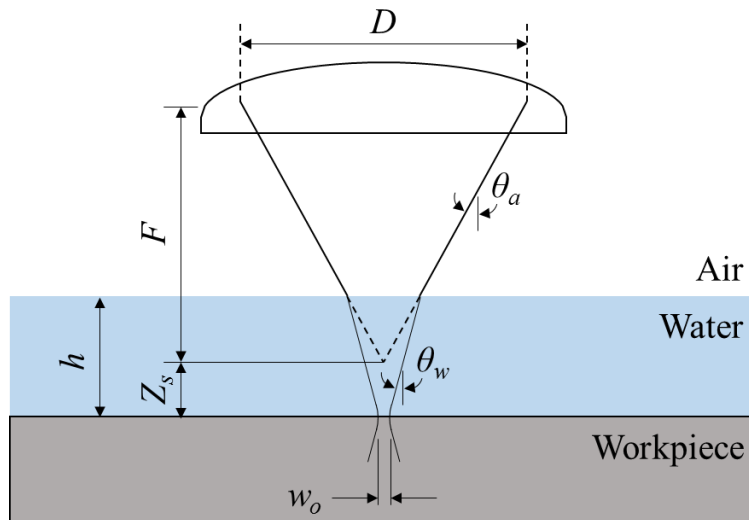


**Fig. 2.2 Refractions of a laser beam through water media.**

In this study, the water was sprayed with a thickness of less than 500  $\mu\text{m}$ . According to the equations, the laser intensity irradiated on the workpiece surface was approximately 99.33% of the initial laser intensity and the focal distance shifted from the initial positions was approximately 12.5  $\mu\text{m}$ . Therefore, it can be deduced that a 500- $\mu\text{m}$ -thickness of water was not thick enough to affect the laser conditions irradiated on the workpiece.

# Chapter 3

## Machining Mechanism investigation

In this chapter, the ablation behaviors of silicon compound ceramics were observed during laser beam machining (LBM) in air and water, which helped to determine the reasons for the different ablation behaviors. To investigate the machining principles in LBM of silicon compound ceramics, the laser beam was irradiated in water and kerosene and the chemical composition analysis on the irradiated surfaces was conducted. Then, how the hydrothermal reaction between the silicon compound ceramics and the water affected the LBM is explained.

### 3.1. Ablation Behavior in Air and Water

Figure 3.1 shows micro-cavities machined by the laser beam in air and water for silicon nitride ( $\text{Si}_3\text{N}_4$ ) and silicon carbide ( $\text{SiC}$ ), respectively. 3 W and 8 W of laser power were applied during LBM of  $\text{Si}_3\text{N}_4$  and  $\text{SiC}$

respectively, and other machining conditions were as follows: 100 times of scan repeat count, 100 mm/s of scan speed, and 50 kHz of nominal pulse repetition rate for both materials. Both ceramics were machined effectively in water, while the materials were not sufficiently removed in air under the same machining conditions. The cross section images, according to the scan repeat count, are shown in Figures 3.2 and 3.3. When both Si<sub>3</sub>N<sub>4</sub> and SiC were ablated in water, the material removal volume of both materials increased markedly with the increasing scan repeat count. In the case of ablation in air, no additional increase of material removal volume was found in either material with the increasing scan repeat count. At the beginning of the process, a recast layer was generated at the irradiated surface by laser ablation. However, further machining was prevented by the accumulation of a recast layer in spite of the increasing scan repeat count. Also, the surface morphologies of both materials were changed due to the accumulation of a recast layer formed during LBM in air.



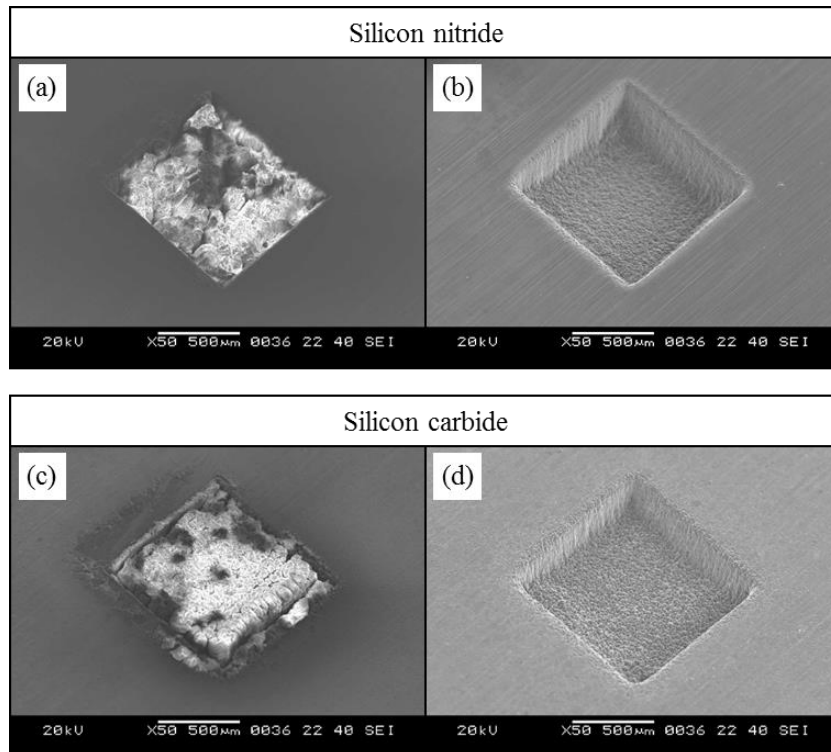


**Fig. 3.1 SEM micrographs of cavities in silicon compound ceramics machined by the laser beam: (a, c) in air, (b, d) in water.**

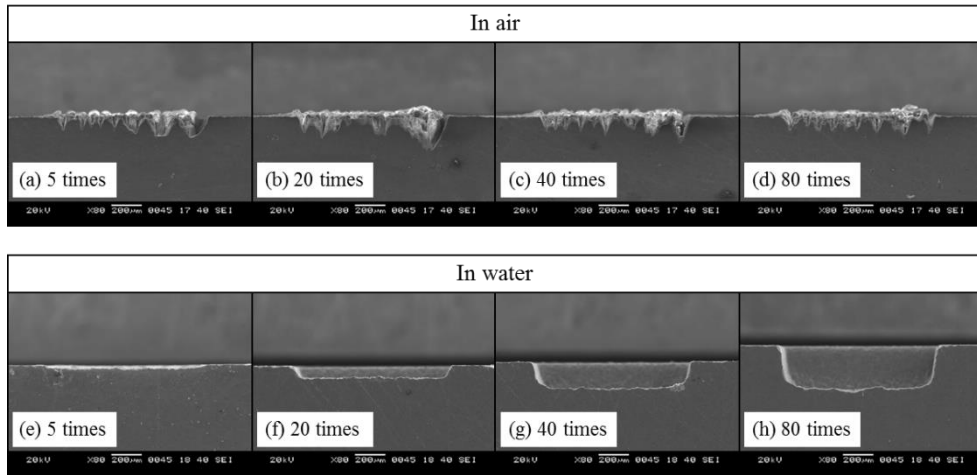


**Fig. 3.2** Cross section views of cavities machined by the laser beam on the  $\text{Si}_3\text{N}_4$  surface according to scan repeat count (3 W of laser power, 100 mm/s of scan speed): (a, b, c, d) in air, (e, f, g, h) in water.

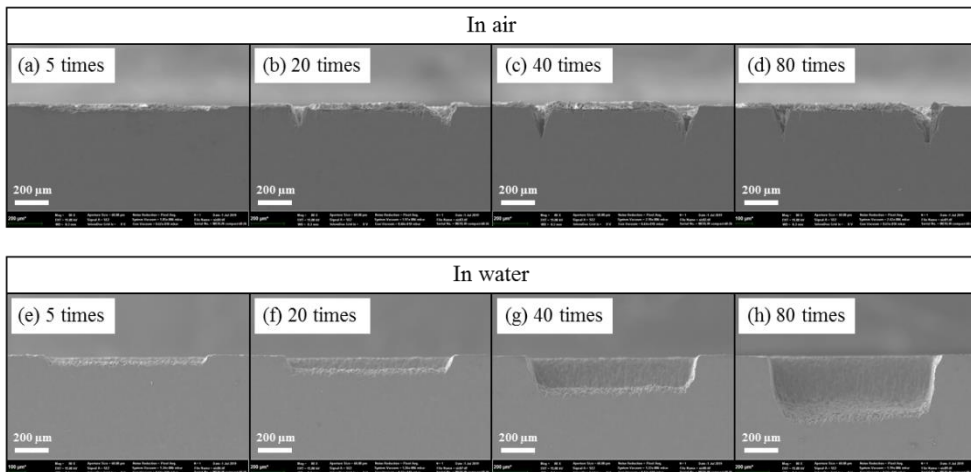


**Fig. 3.3** Cross section views of cavities machined by the laser beam on the SiC surface according to scan repeat count (8 W of laser power, 100 mm/s of scan speed): (a, b, c, d) in air, (e, f, g, h) in water.

Also, a noticeable increase of oxygen was measured at the surface machined in air, although little chemical composition change was observed at the surface machined in water according to the EDS results. Laser irradiated surfaces of  $\text{Si}_3\text{N}_4$ , measurement sites for EDS analysis, are shown in Figure 3.4. The EDS results for elemental compositions of  $\text{Si}_3\text{N}_4$  before and after laser beam machining in different mediums are shown in Table 3.1. After LBM in air, the atomic percentage of oxygen increased noticeably from 9.53% to 63.37%, while few percentages of the element nitrogen was observed. However, the changes in elemental compositions at the machined surface after LBM in water were negligible. The elements carbon, aluminum, and titanium, which came from binding materials used in the sintering process, were not noticeably changed after laser ablation in either air or water.

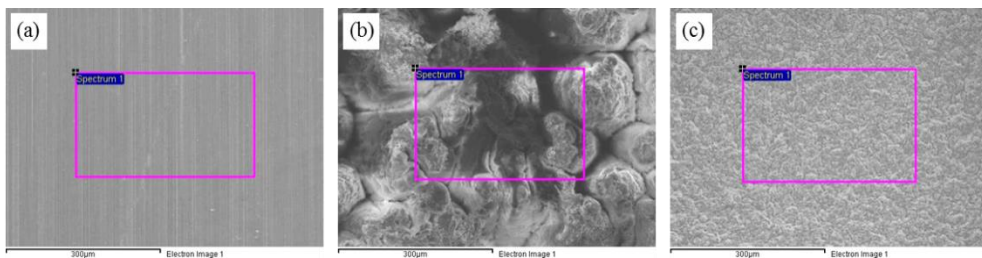


**Fig. 3.4 SEM micrographs of  $\text{Si}_3\text{N}_4$  surfaces in different laser ablation conditions: (a) reference  $\text{Si}_3\text{N}_4$  surface; (b) laser ablation in air; (c) laser ablation in water**

**Table 3.1 EDS results for elemental compositions of Si<sub>3</sub>N<sub>4</sub> before and after laser ablation**

Samples (silicon nitride)	Si (atomic%)	N (atomic%)	O (atomic%)	C, Al, Ti (atomic%)
Before laser ablation	30.71	45.74	<u>9.53</u>	14.02
After laser ablation in air	22.47	~0	<u>63.37</u>	14.15
After laser ablation in water	27.88	41.16	<u>15.96</u>	14.9

The elemental compositions of SiC also showed similar results to Si<sub>3</sub>N<sub>4</sub> (Table 3.2). Laser irradiated surfaces of SiC, measurement sites for EDS analysis, are shown in Figure 3.5. After LBM in air, the atomic percentage of oxygen increased from 2.88% to 64.27%, whereas the chemical compositions of the surface machined in water did not change significantly. The EDS maps of oxygen and silicon on the Si<sub>3</sub>N<sub>4</sub> and SiC surfaces machined in air are shown in Figure 3.6 and 3.7, respectively. The EDS maps indicate the recast layer is composed of oxygen and silicon.

**Table 3.2 EDS results for elemental compositions of SiC before and after laser ablation**

Samples (silicon carbide)	Si (atomic%)	C (atomic%)	O (atomic%)
Before laser ablation	37.25	59.87	<u>2.88</u>
After laser ablation in air	22.54	13.20	<u>64.27</u>
After laser ablation in water	33.60	63.72	<u>2.68</u>

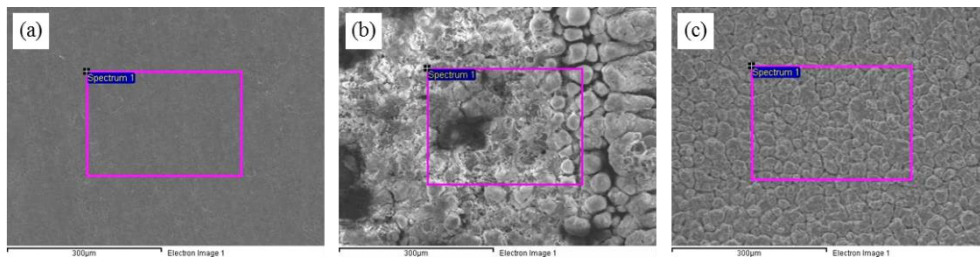


**Fig. 3.5 SEM micrographs of SiC surfaces in different laser ablation conditions: (a) reference SiC surface; (b) laser ablation in air; (c) laser ablation in water**

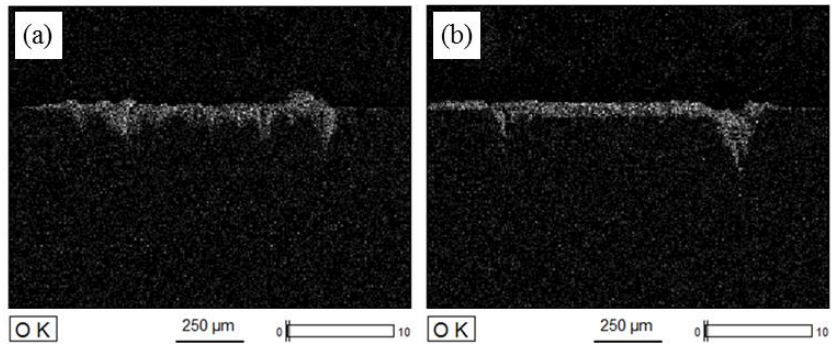


**Fig. 3.6 EDS map analysis of oxygen on the cross section surfaces ablated by the laser in air: (a) Si<sub>3</sub>N<sub>4</sub>, (b) SiC.**

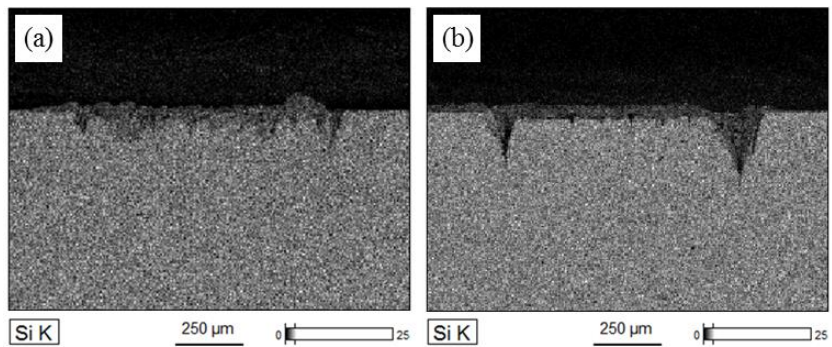


**Fig. 3.7 EDS map analysis of silicon on the cross section surfaces ablated by the laser in air: (a) Si<sub>3</sub>N<sub>4</sub>, (b) SiC.**

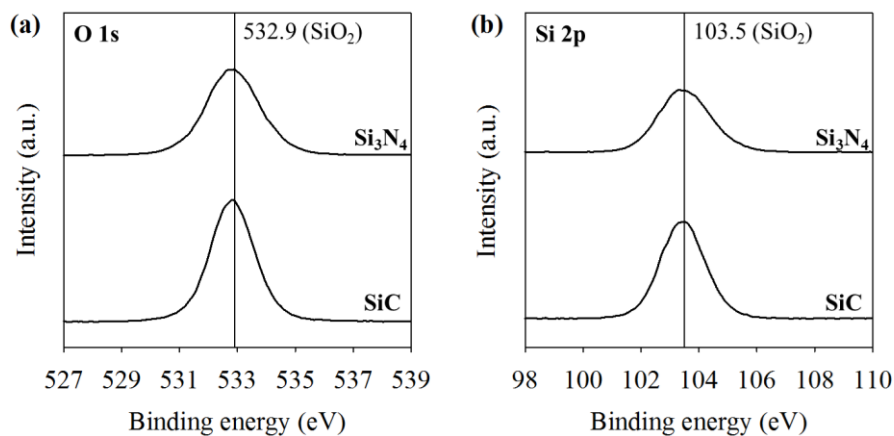


**Fig. 3.8 XPS spectra for surfaces of Si<sub>3</sub>N<sub>4</sub> and SiC machined by the laser beam in air: (a) O 1s, (b) Si 2p.**

To investigate the reason for the increase in oxygen, XPS analysis was conducted (Figure 3.8). Both Si<sub>3</sub>N<sub>4</sub> and SiC surfaces ablated in air exhibited an O 1s peak at a binding energy of 532.9 eV and a Si 2p peak at a binding energy of 103.5 eV, which is identical to the binding energy of silicon dioxide (SiO<sub>2</sub>). This suggests that both Si<sub>3</sub>N<sub>4</sub> and SiC were oxidized to SiO<sub>2</sub> by laser ablation in air.

When silicon compound ceramics were ablated in air, the materials were oxidized to SiO<sub>2</sub> and accumulated on the laser irradiated surfaces without further removal of the materials. Table 3.3 shows thermodynamic properties and measured absorbance values of SiO<sub>2</sub>, Si<sub>3</sub>N<sub>4</sub>, and SiC. The absorbance was

measured at wavelength of 1064 nm same with wavelength used in LBM. Since, specific heat capacity, sublimation point, and bond energy of  $\text{SiO}_2$  is higher than that of  $\text{Si}_3\text{N}_4$  and  $\text{SiC}$ , it can be deduced that more energy is needed to ablate  $\text{SiO}_2$  compared with  $\text{Si}_3\text{N}_4$  and  $\text{SiC}$ . In addition, absorbance of  $\text{SiO}_2$  at 1064 nm was lower than that of  $\text{Si}_3\text{N}_4$  and  $\text{SiC}$ . Therefore, negligible change in the ablated volume of the materials in air can be explained by interference with the removal of non-oxidized materials by an accumulated  $\text{SiO}_2$  layer. However, when silicon compound ceramics were ablated in water, a  $\text{SiO}_2$  layer was not found and no significant changes in chemical composition were observed in the machined area. As there was no  $\text{SiO}_2$  to interfere with the material removal, effective LBM in water would have been possible.



**Table 3.3 Thermodynamic properties and measured absorbance values of Si<sub>3</sub>N<sub>4</sub>, SiC, and SiO<sub>2</sub> [47–50].**

Materials	Si <sub>3</sub> N <sub>4</sub>	SiC	SiO <sub>2</sub>
Specific heat capacity [J/kg·K]	510-650	680-800	1000
Sublimation point [°C]	1900	2527	2950
Bond energy [kJ/mol]	435	439	798
Absorbance at 1064 nm wavelength [%]	88.9	82.1	74.3

### **3.2. Assist of Hydrothermal Reaction during Underwater LBM**

Previous researches found that silicon compound ceramics, including Si<sub>3</sub>N<sub>4</sub> and SiC, are hydrothermally corroded in water above 200°C [40–44]. As the temperature of water increases, the silicon compound ceramics are oxidized to SiO<sub>2</sub>, which tends to dissolve in water. Because the temperature where the hydrothermal reaction is initiated (200°C) was lower than the temperature where Si<sub>3</sub>N<sub>4</sub> and SiC were ablated, reactions between the materials and water inevitably occurred.

Hydrothermal reaction between water and silicon compound ceramics is spontaneous process according to a Gibbs free energy calculation. The formulas of the Gibbs free energy are as follows:

$$\Delta H = \Sigma \Delta H_f^0(\text{products}) - \Sigma \Delta H_f^0(\text{reactants})$$

$$\Delta S = \Sigma S^0(\text{products}) - \Sigma S^0(\text{reactants})$$

$$\Delta G = \Delta H - T\Delta S$$

$\Delta H$ ,  $\Delta H_f^0$ ,  $\Delta S$ ,  $S^0$ ,  $\Delta G$ , and  $T$  are the enthalpy change of reaction, the standard enthalpy of formation, the entropy change of reaction, the standard molar entropy, the Gibbs free energy change of reaction, and the absolute temperature, respectively. The standard thermodynamic values of the elements in hydrothermal reaction are summarized in table 3.4. The spontaneity of the reaction is determined by the sign of the Gibbs free energy change of reaction. When the Gibbs free energy is a negative number, the reaction is spontaneous. As the enthalpy change of the reaction is negative, and the entropy change of reaction is positive, the sign of the Gibbs free energy change is negative regardless of temperature, indicating the reaction is spontaneous. All of the reactions in hydrothermal reaction of silicon compound ceramics always have a negative Gibbs free energy change

regardless of temperature. Therefore, the hydrothermal reaction of silicon compound ceramics can be determined as a spontaneous process.

**Table 3.4 Standard thermodynamic values of the elements in hydrothermal reaction at 25°C [51,52].**

Substance	$\Delta H_f^0$ [kJ/mol]	$S^0$ [J/mol·K]
Si <sub>3</sub> N <sub>4</sub> (s)	-743.5	113.0
SiC (s)	-71.6	16.5
H <sub>2</sub> O (l)	-285.8	69.9
CH <sub>4</sub> (g)	-74.9	186.3
NH <sub>3</sub> (g)	-46.1	192.3
SiO <sub>2</sub> (amorphous)	-903.5	46.9
H <sub>2</sub> SiO <sub>3</sub> (s)	-1188.7	133.9

High temperature induced by laser beam also accelerates the hydrothermal reaction during the process. At room temperature, hydrothermal reaction is not observed because of low reaction rate. For a reaction to occur, the activation energy is necessary to break the bond of the molecules. An increase in temperature increases the number of molecules with higher energy than the

activation energy. Consequently, temperature increase accelerates reaction rate. Therefore, the hydrothermal reaction sufficiently occurs during the underwater LBM, while the hydrothermal reaction is not observed at room temperature. Figure 3.9 shows a reaction coordinate diagram for the hydrothermal reaction of silicon compound ceramics.

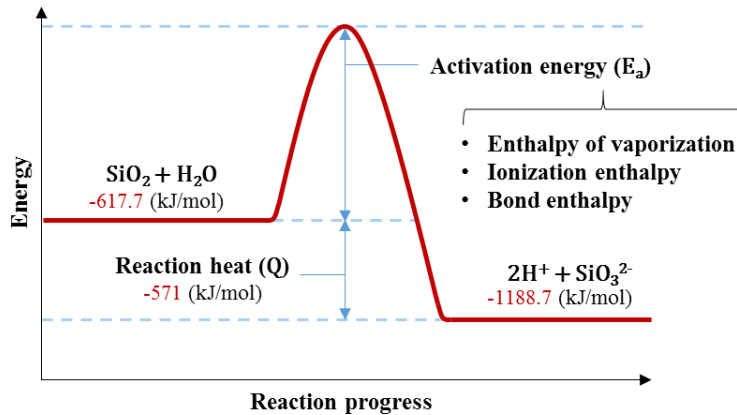


**Fig. 3.9** Reaction diagram for the hydrothermal reaction of silicon compound ceramics.

A reaction rate of the hydrothermal reaction during the underwater LBM was calculated. A reaction rate can be defined by the concentration of the reactant and the rate constant ( $k$ ). The formulas of the reaction rate and rate constant is as follows:

$$r = k(T)[SiO_2]^m[H_2O]^n$$

$$k = Ae^{-\frac{E_a}{RT}} \quad (4.1)$$

$$\ln(k) = -\frac{E_a}{R}\left(\frac{1}{T}\right) + \ln(A) \quad (4.2)$$

$A$ ,  $E_a$ ,  $R$ , and  $T$  are the frequency factor, the activation energy, the gas constant, and the absolute temperature, respectively. Since the concentration of the reactant is almost constant due to the continuous supply of water by flushing, the reaction rate is determined by the rate constant. The rate constant can be calculated by the Arrhenius equation as shown in Formula 4.1. Since the frequency factor, the activation energy, and the gas constant are constant, the logarithm of the rate constant is a linear function of an inverse of the absolute temperature, as shown in Formula 4.2.

Previous research found the rate constant of the hydrothermal reaction as a function of the temperature. Figure 3.10 shows the Arrhenius plot of the

hydrothermal reaction of  $\text{Si}_3\text{N}_4$ . The rate constant of hydrothermal reaction during the underwater LBM was estimated by the Arrhenius plot. In calculation, activation energy is 108 kJ/mol [40]. Since a melting point of  $\text{Si}_3\text{N}_4$  is about 1900°C, the temperature is assumed as 1900°C. As a result, the rate constant at 1900°C is calculated as  $2.71 \times 10^5$ . As the calculated rate constant at 200°C is about  $1.25 \times 10^{-4}$ , the rate constant at 1900°C increased  $2.15 \times 10^9$  times, compared to the rate constant at 200°C. Since a reaction rate is proportional to the rate constant, the reaction rate of hydrothermal reaction is sufficient during the underwater LBM.

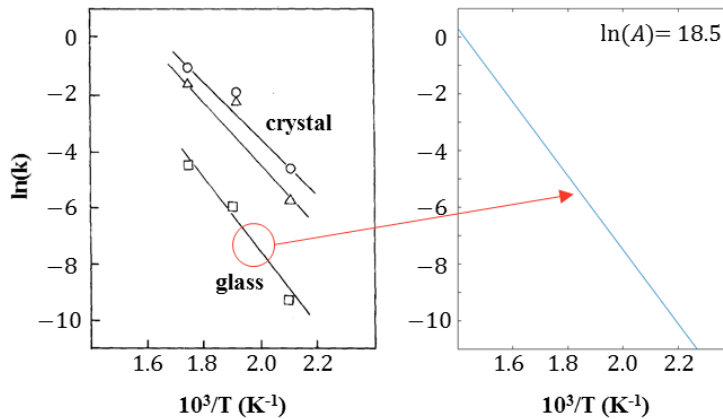


**Fig. 3.10** Reaction diagram for the hydrothermal reaction of silicon compound ceramics [40].

To confirm the effects of hydrothermal reaction on the removal of SiO<sub>2</sub>, silicon compound ceramics were irradiated in water and kerosene. After forming the SiO<sub>2</sub> on the material surfaces by laser ablation in air, the laser beam was re-irradiated in water and kerosene to confirm the hydrothermal reaction between water and SiO<sub>2</sub>. The laser beam in a heated condition, which is below the machining condition (i.e., laser power of 0.5 W and scan repeat count of 1), irradiated the surfaces covered with SiO<sub>2</sub>. A schematic diagram of the experiments to investigate the chemical effects of water media on the removal of SiO<sub>2</sub> is shown in Figure 3.11.

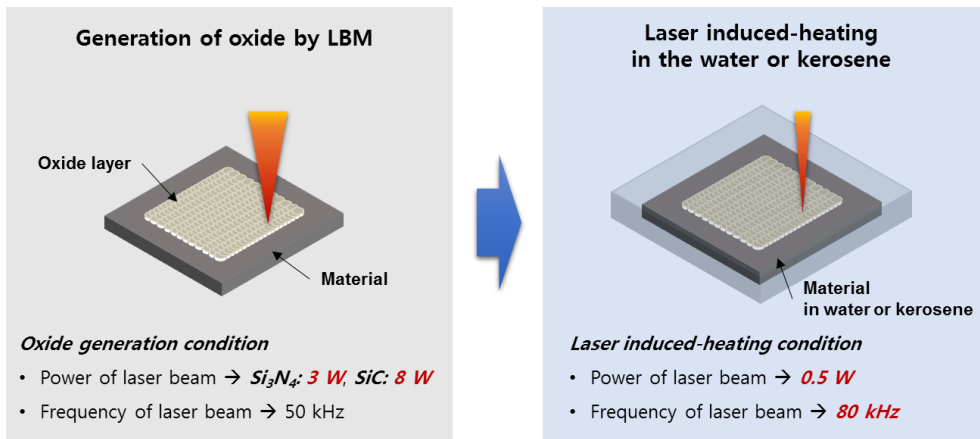


**Fig. 3.11 Schematic diagram of the experiments to investigate the chemical effects of water on the removal of SiO<sub>2</sub>.**

The EDS results for the elemental composition of  $\text{Si}_3\text{N}_4$  and  $\text{SiC}$  irradiated by the laser in water and kerosene are shown in Tables 3.5 and 3.6, respectively. Also, laser irradiated surfaces of  $\text{Si}_3\text{N}_4$  and  $\text{SiC}$ , measurement sites for EDS analysis, are shown in Figure 3.12 and 3.13, respectively. After laser irradiation in water, the atomic percentage of oxygen decreased, while that of the surfaces irradiated in kerosene did not noticeably change. The oxygen atomic percentage of both materials irradiated in water decreased by approximately one third. In contrast, no significant difference was found in the oxygen atomic percentage of either material before or after laser irradiation in kerosene. Also, when the laser beam was irradiated in water the surface morphology was changed by the removal of the recast layer that had accumulated on the ablated surfaces, as shown in Figure 3.12 and 3.13. However, little change in surface morphology was observed after laser irradiation in kerosene compared with that of the silicon compound ceramics in which the  $\text{SiO}_2$  layer was formed in air.



**Table 3.5 EDS results for elemental compositions of Si<sub>3</sub>N<sub>4</sub> before and after laser ablation**

Samples (silicon nitride)	Si (atomic%)	N (atomic%)	O (atomic%)	C, Al, Ti (atomic%)
Laser irradiation in water after laser ablation in air	28.74	35.34	<u>19.10</u>	16.82
Laser irradiation in kerosene after laser ablation in air	23.06	~0	<u>63.56</u>	13.39

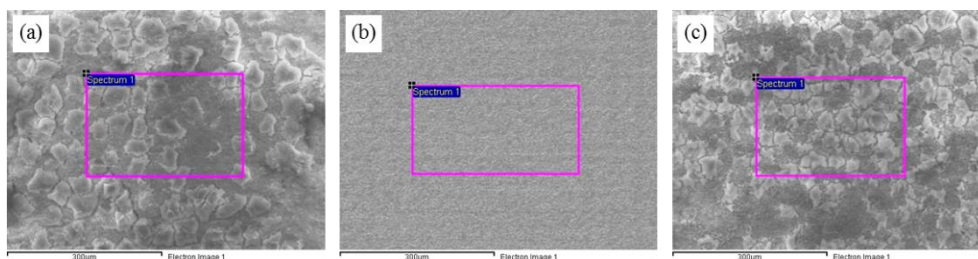


**Fig. 3.12 SEM micrographs of Si<sub>3</sub>N<sub>4</sub> surfaces in different laser ablation conditions: (a) laser ablation in air; (b) laser irradiation in water after laser ablation in air; (c) laser irradiation in kerosene after laser ablation in air.**

**Table 3.6 EDS results for elemental compositions of SiC before and after laser ablation**

Samples (silicon carbide)	Si (atomic%)	C (atomic%)	O (atomic%)
Laser irradiation in water after laser ablation in air	37.05	42.66	<u>20.29</u>
Laser irradiation in kerosene after laser ablation in air	16.04	16.64	<u>58.10</u>

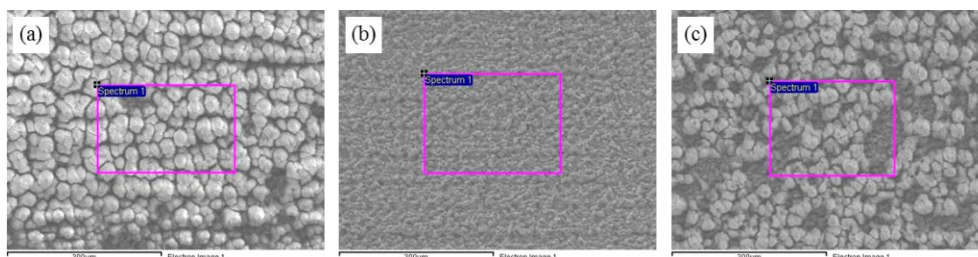


**Fig. 3.13 SEM micrographs of SiC surfaces in different laser ablation conditions: (a) laser ablation in air; (b) laser irradiation in water after laser ablation in air; (c) laser irradiation in kerosene after laser ablation in air.**

In water, the  $\text{SiO}_2$  generated in air was removed by laser irradiation even when the laser conditions were not enough to ablate the materials. In contrast,  $\text{SiO}_2$  was not removed in kerosene with the same laser conditions. This was due to the dissolution of  $\text{SiO}_2$  in water by hydrothermal reaction induced by laser beam irradiation. It can be deduced that increasing temperature caused by laser irradiation promoted the hydrothermal reaction.

As a result, the material removal mechanism in underwater LBM of silicon compound ceramic can be explained as follows. In LBM of silicon compound ceramics, a recast layer composed of  $\text{SiO}_2$  interferes with the material removal, and decreases efficiency of the process. In underwater LBM of silicon compound ceramics, however, there was no  $\text{SiO}_2$  to interfere with the effective ablation of the silicon compound ceramics because of the hydrothermal reaction. Therefore, silicon compound ceramics can be machined continuously in water. The schematic diagram for material removal mechanism during LBM of silicon compound ceramics in air and water is shown in Figure 3.14.

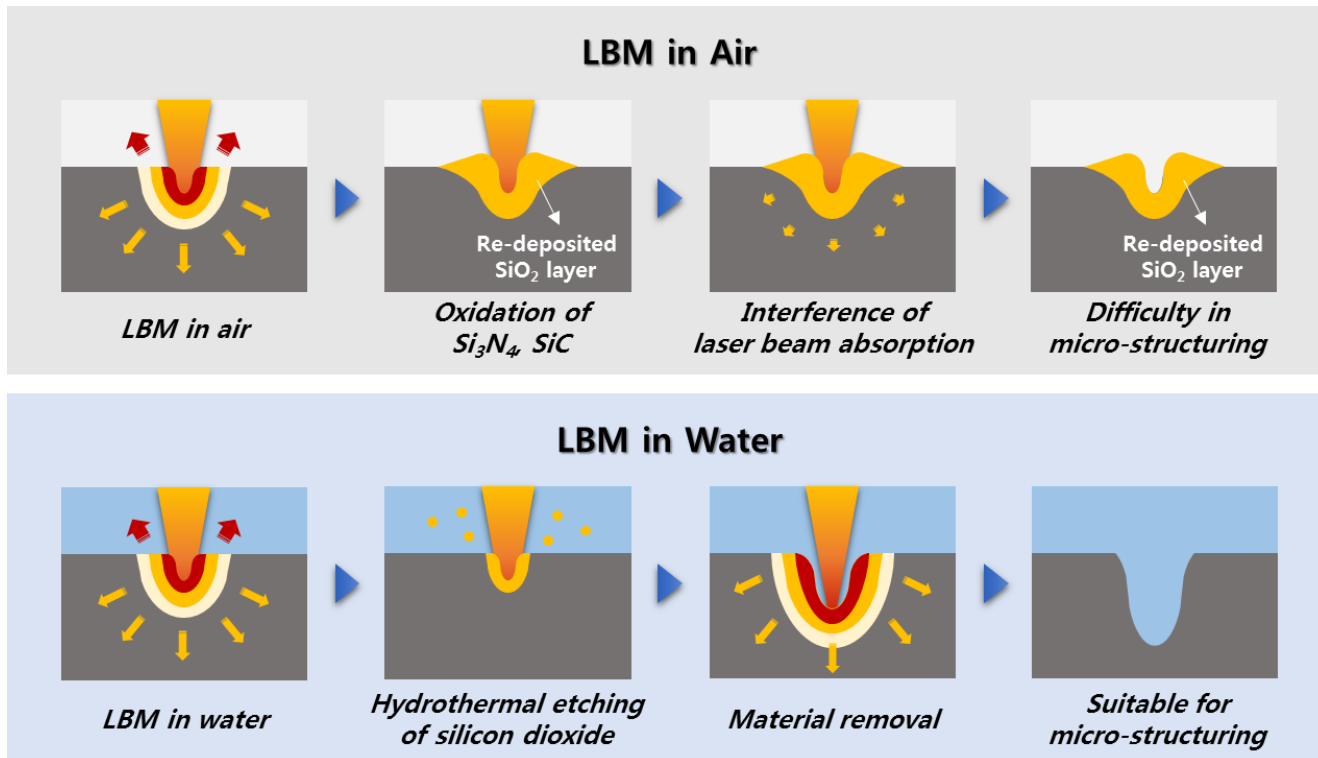


**Fig. 3.14** Schematic diagram for material removal mechanism during LBM of silicon compound ceramics in air and water.

# Chapter 4

## Machining Characteristics

To investigate the effect of the laser beam in water on the ablation of silicon compound ceramics, the grooves were machined by LBM in air and water. First, the effect of the flow rate of water on the hydrothermal reactive LBM of silicon compound ceramics was investigated. Then, a parametric study of the effect of laser conditions such as laser power, scan repeat count, and scan speed on the machining was investigated. Consequently, dimensions of grooves machined by LBM in air and water were compared with respect to the laser conditions and proper laser conditions for micro-structuring were suggested.

## 4.1. Effect of Flow rates of Water

As the flow rate of water increases, a deeper and narrower groove can be machined in both  $\text{Si}_3\text{N}_4$  and  $\text{SiC}$ . Figure 4.1 shows the depth and width of the channel with respect to the flow rate of water. The width of the grooves was measured at the top surface of the groove. In both silicon compound ceramics materials, the depth increased and the width decreased with the increased flow rate of water. In Figure 4.2 and 4.3, the cross section of grooves in different water flow rates is shown. At a 2 ml/s flow rate, the edges of the groove entrance were damaged compared to that machined with a 6 ml/s in both materials. When the water flow rate was not enough to flush away the debris and bubbles, the debris absorbed the laser beam energy instead of the workpiece and disturbed the deep groove machining. The bubbles also scattered the laser beam, which damaged and widened the entrance of the groove. However, the effect of the flow rate on the dimension of the groove gradually decreased with the increasing flow rate. The depth and width of the grooves converged over a flow rate of 5 ml/s in  $\text{Si}_3\text{N}_4$  and  $\text{SiC}$ . Once the flow rate was sufficient to remove the debris and bubbles, the increased flow rate did not have a further effect on machining.

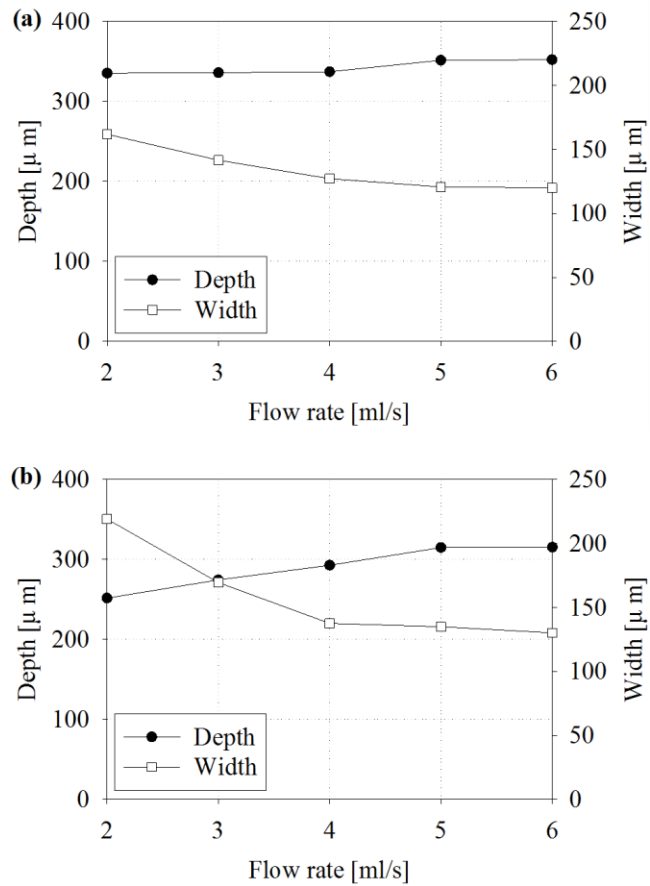


**Fig. 4.1** The relation between dimensions of channel and flow rate of water when machining silicon compound ceramics by laser beam in water: (a) Si<sub>3</sub>N<sub>4</sub>, (b) SiC.

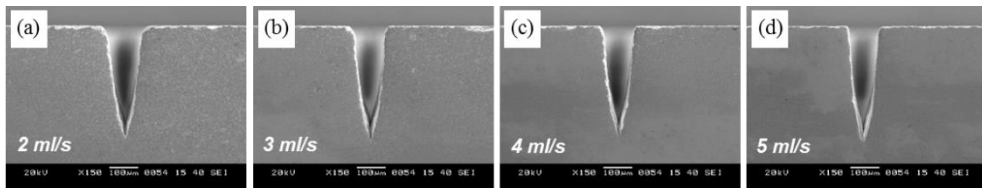


**Fig. 4.2** Cross section views of micro-channels in Si<sub>3</sub>N<sub>4</sub> obtained by laser beam machining in water with different flow rate of water: (a) 2 ml/s; (b) 3 ml/s; (c) 4 ml/s; (d) 5 ml/s.

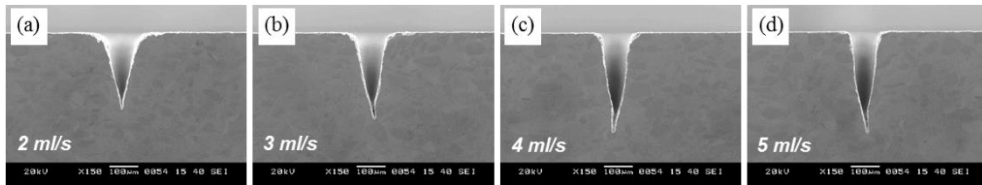


**Fig. 4.3** Cross section views of micro-channels in SiC obtained by laser beam machining in water with different flow rate of water: (a) 2 ml/s; (b) 3 ml/s; (c) 4 ml/s; (d) 5 ml/s.



## **4.2. Effect of Laser Conditions**

In this section, the effects of laser conditions on the hydrothermal reactive LBM of silicon compound ceramics were investigated such as laser power, scan repeat count, and scan speed. Also, proper laser conditions for micro-structuring were suggested.

### **4.2.1. Laser Power**

In both the LBM of silicon compound ceramics in air and water, the depth and width of the grooves increased with increasing laser power as shown in Figure 4.4 and 4.5. Although the tendency with respect to laser power in both air and water was similar, the depth and width significantly increased in the water compared with the air due to the hydrothermal reaction. The entrance width of machined groove can be controlled by changing laser power condition. In this research, a micro-structuring of silicon compound ceramics on a scale of 100  $\mu\text{m}$  is conducted using the hydrothermal reactive LBM. On  $\text{Si}_3\text{N}_4$ , the entrance width at the laser power of 6 W was about 100  $\mu\text{m}$ . On SiC, the entrance width of machined groove at the laser power of 8 W was about 100  $\mu\text{m}$ . Therefore, 6 W and 8 W of laser power were set as basic laser

power condition for  $\text{Si}_3\text{N}_4$  and  $\text{SiC}$ , respectively. The cross section of the grooves obtained by LBM in air and water in  $\text{Si}_3\text{N}_4$  and  $\text{SiC}$  are shown in Figure 4.6 and 4.7, respectively. The grooves were machined at scan repeat count of 2000 times and scan speed of 100 mm/s.

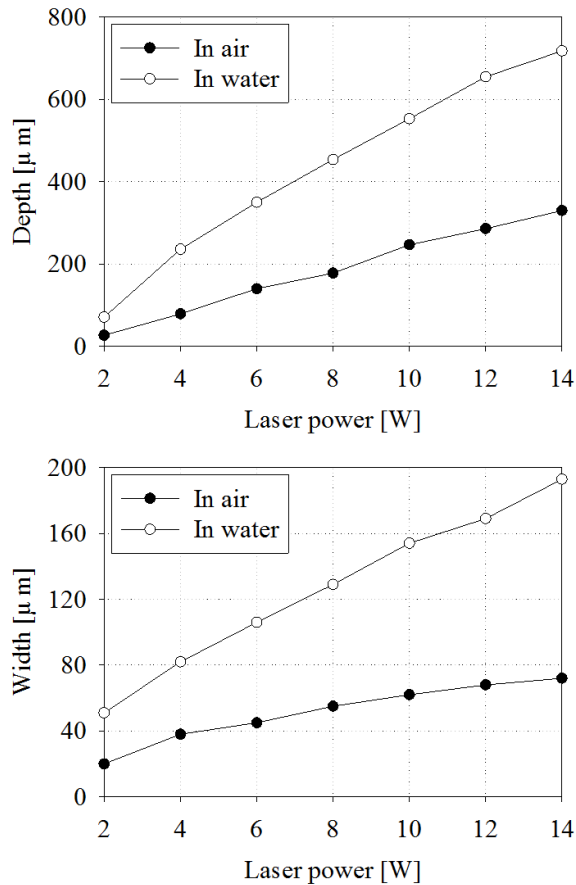


**Fig. 4.4** Tendency of depth and width of grooves machined in air and water on the  $\text{Si}_3\text{N}_4$  surfaces according to laser power.

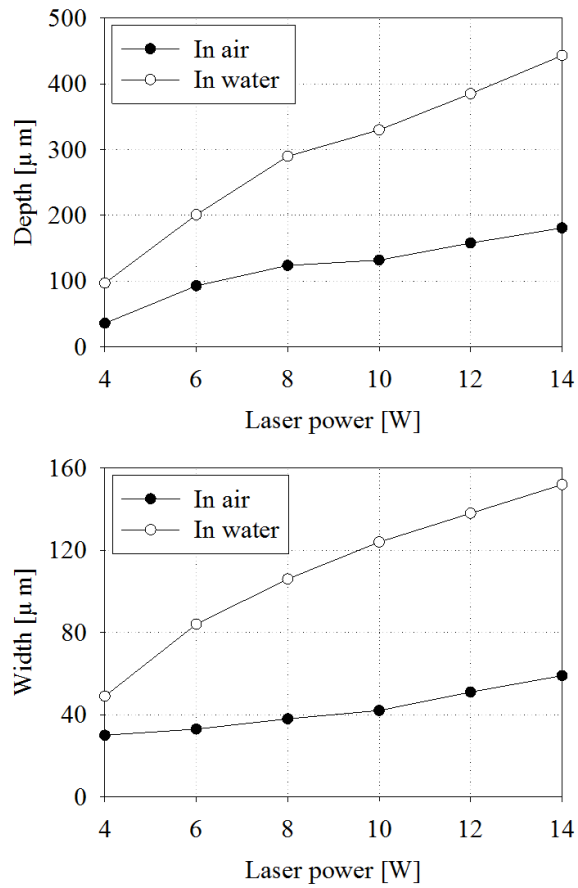


**Fig. 4.5** Tendency of depth and width of grooves machined in air and water on the SiC surfaces according to laser power.

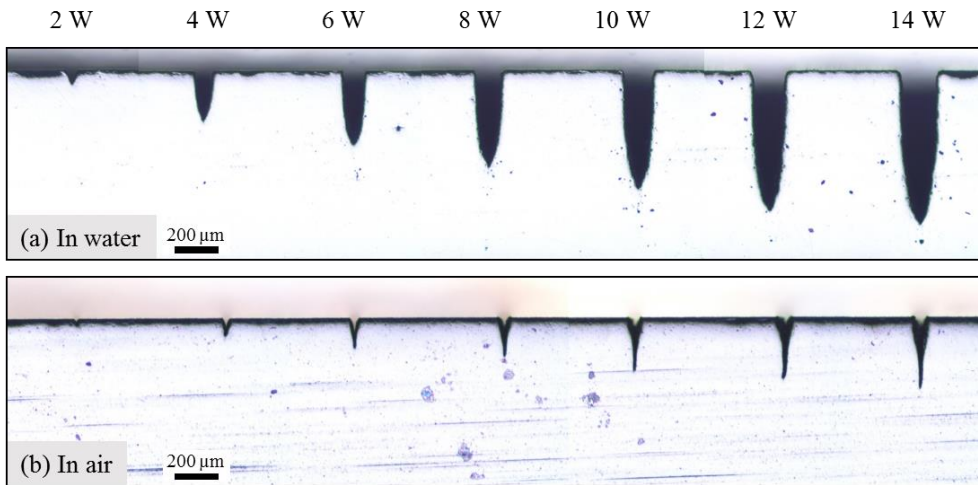


**Fig. 4.6** Cross section views of micro-channels in Si<sub>3</sub>N<sub>4</sub> obtained by laser beam machining with different laser power: (a) in water, (b) in air.

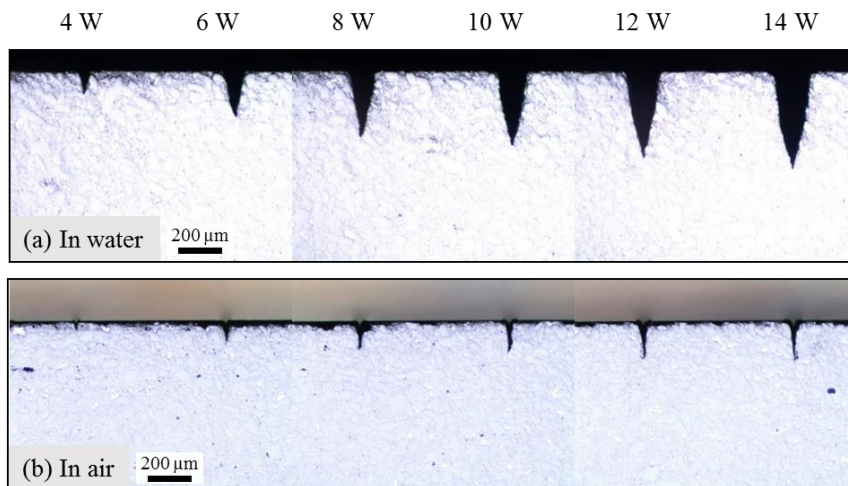


**Fig. 4.7** Cross section views of micro-channels in SiC obtained by laser beam machining with different laser power: (a) in water, (b) in air.

The width expansion with increasing laser power can be explained by a Gaussian distribution of laser intensity and a threshold power intensity, as shown in Figure 4.8 and 4.9, respectively. The mathematical form of the Gaussian distribution of laser intensity is as follows:

$$I(r) = I_0 e^{\left\{-2\left(\frac{r}{w_0}\right)^2\right\}}$$

$I$ ,  $I_0$ ,  $r$ , and  $w_0$  are the laser intensity, the maximum laser intensity, the radial distance from the beam center, and the radius of the spot size, respectively. The threshold power intensity is the minimum of laser intensity for ablating material. In this experiment, SiC was not ablated at the laser power of 2 W, while Si<sub>3</sub>N<sub>4</sub> was able to be machined at the same laser power, because the threshold laser intensity of SiC is higher than that of Si<sub>3</sub>N<sub>4</sub>. As increasing laser power, the maximum laser intensity increases, while the released beam diameter from laser source is not changed. Therefore, a reactive diameter over the threshold laser intensity increases with increasing laser power. The reactive diameter over the threshold laser intensity can be calculated as follows:

$$I_T(r) = I_a e^{-2\left(\frac{r}{w_0}\right)^2}$$

$$D^2 = \frac{1}{2} w_0^2 \ln \frac{I_a}{I_T}$$

$$D = w_0 \sqrt{\frac{1}{2} \ln \left( \frac{I_a}{I_T} \right)}$$

$I_a$ ,  $I_T$ , and  $D$  are the applied laser intensity, the threshold laser intensity, and the reactive diameter, respectively. Therefore, the width of machined groove increased with increasing laser power, because the reactive diameter increases with increasing laser power.

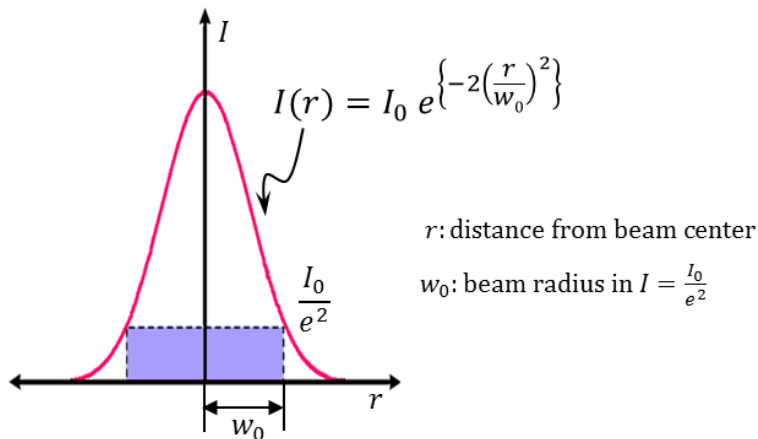


**Fig. 4.8 Laser intensity graph with a Gaussian distribution.**

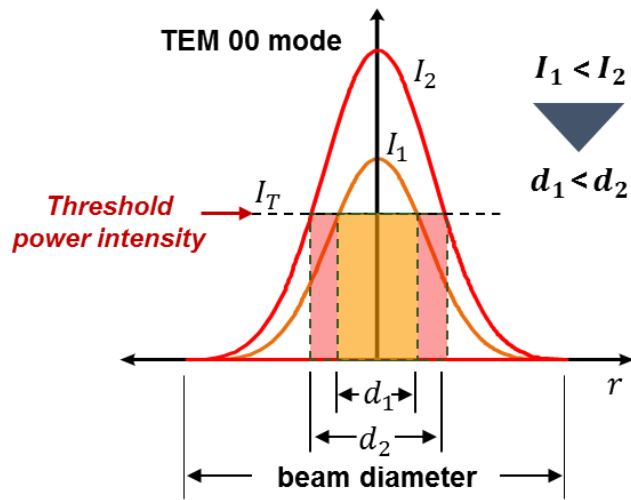
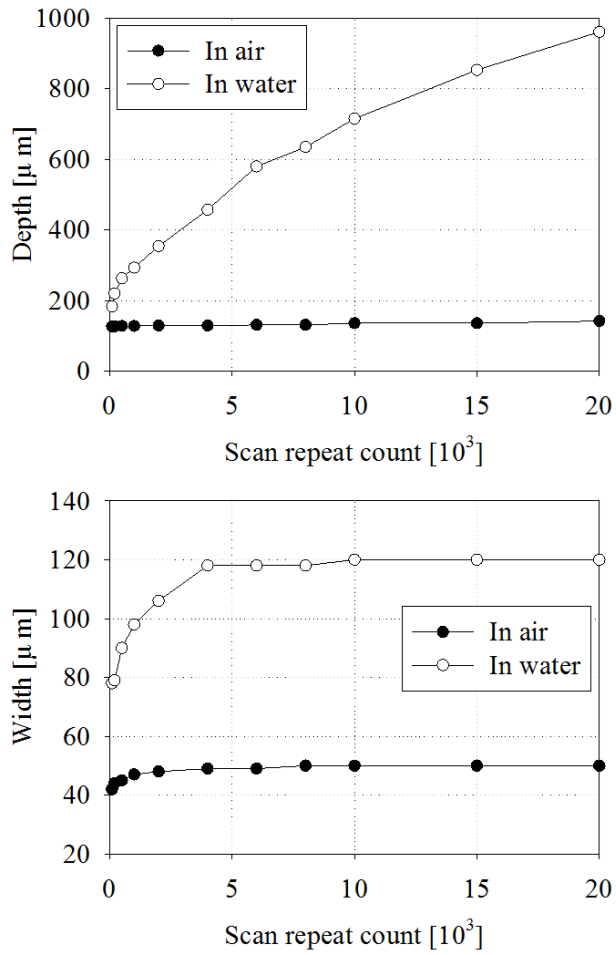


**Fig. 4.9 Principle of width expansion with increasing laser power.**

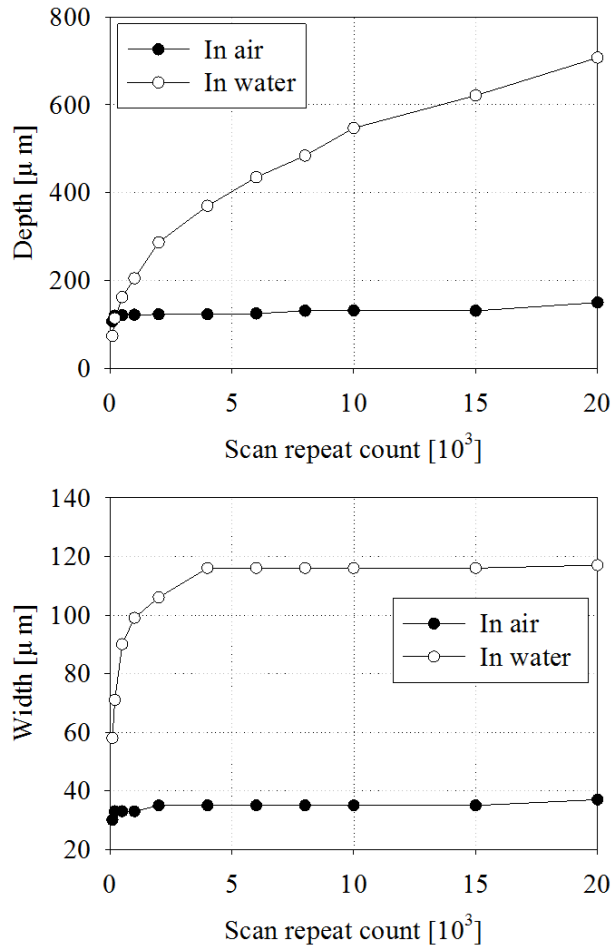
## 4.2.2. Scan Repeat Count

Figure 4.10 and 4.11 show the depth and width of the  $\text{Si}_3\text{N}_4$  and  $\text{SiC}$  grooves machined in air and water with an increasing scan repeat count. For the LBM in water, the depth increased with the increasing scan repeat count. There was no change in depth with increasing scan repeat count when silicon compound ceramics were machined in air. The silicon compound ceramics materials were able to be ablated continuously by laser beam in water because there was no oxide layer to interfere with the laser absorption by hydrothermal reaction. However, when the materials were machined in the air, the generated oxide layer interfered with the sequential ablation of materials. In both air and water the widths of the grooves converged due to the constant spot size of the laser beam. The cross section of the grooves obtained by LBM in air and water in  $\text{Si}_3\text{N}_4$  and  $\text{SiC}$  are shown in Figure 4.12 and 4.13, respectively. The grooves in  $\text{Si}_3\text{N}_4$  and  $\text{SiC}$  were machined at laser power of 6 W and 8 W respectively, at scan speed of 100 mm/s.





**Fig. 4.10** Tendency of depth and width of grooves machined in air and water on the  $\text{Si}_3\text{N}_4$  surfaces according to scan repeat count.



**Fig. 4.11** Tendency of depth and width of grooves machined in air and water on the SiC surfaces according to scan repeat count.

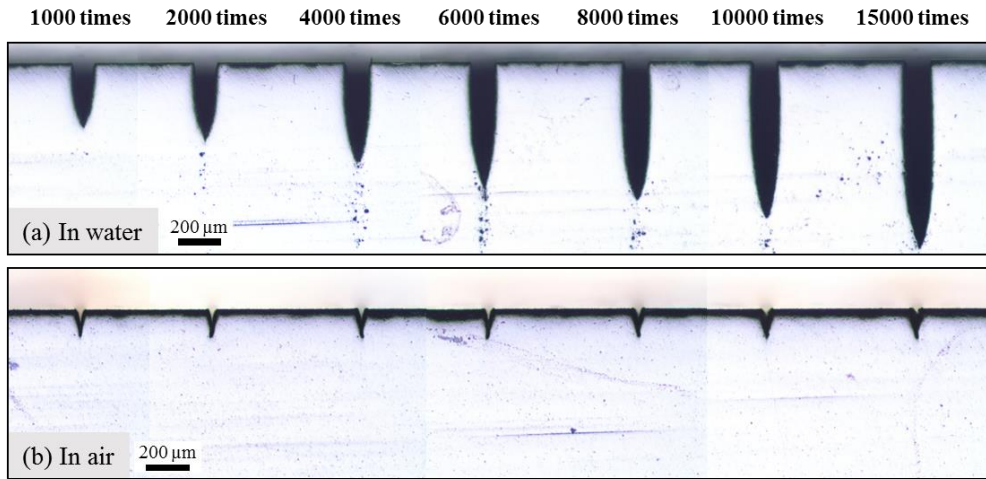


**Fig. 4.12** Cross section views of micro-channels in Si<sub>3</sub>N<sub>4</sub> obtained by laser beam machining with different scan repeat count: (a) in water, (b) in air.

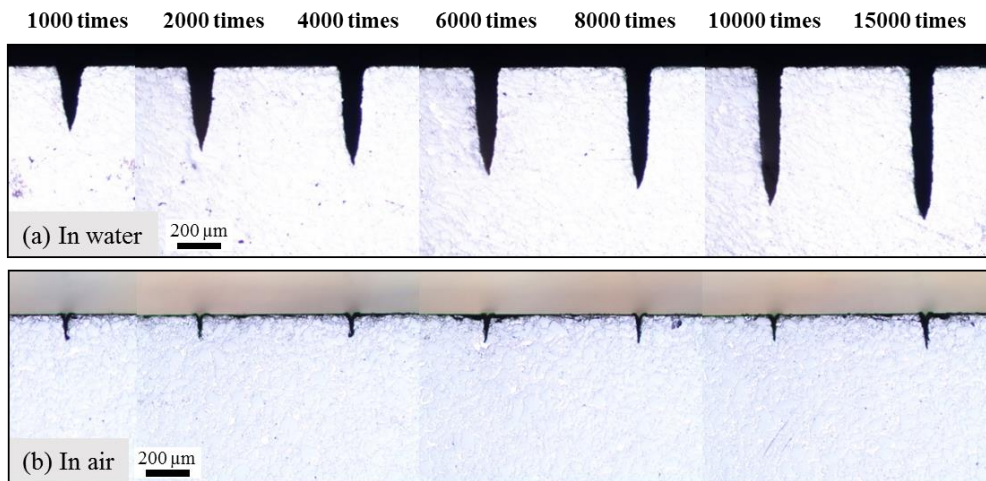


**Fig. 4.13** Cross section views of micro-channels in Si<sub>3</sub>N<sub>4</sub> obtained by laser beam machining with different scan repeat count: (a) in water, (b) in air.

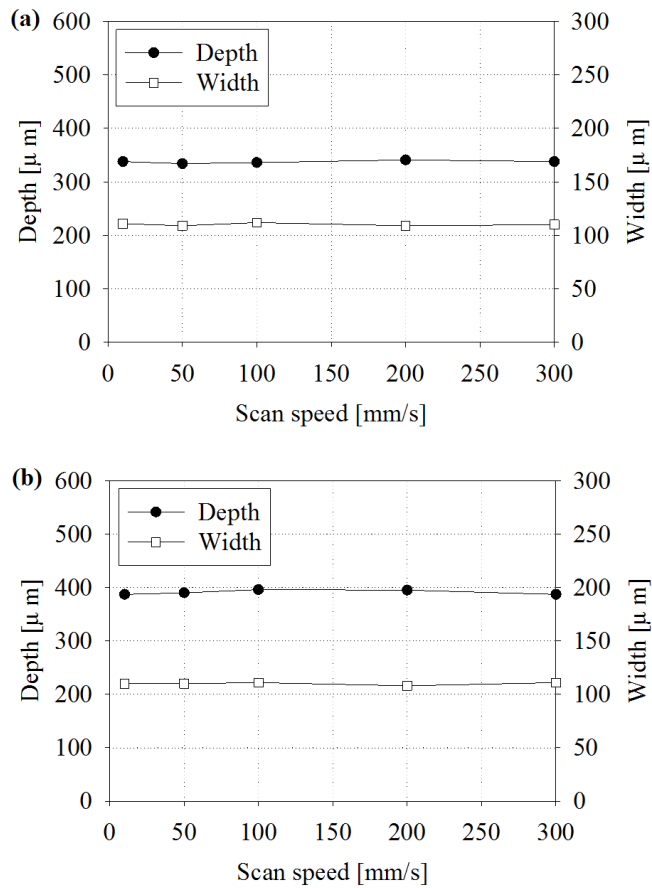
### 4.2.3. Scan Speed

The scan speed did not influence the dimensions of the machined grooves between 10 mm/s and 300 mm/s of the equal scan duration (60 sec). Figure 4.14 shows the relation between the dimensions of grooves and the scan speed when the materials were machined in water. The cross section of the grooves obtained by LBM in air and water in Si<sub>3</sub>N<sub>4</sub> and SiC are shown in Figure 4.15. The grooves in Si<sub>3</sub>N<sub>4</sub> and SiC were machined at laser power of 6 W and 8 W, respectively, and at scan duration of 60 second. At an equal scan duration, there was no significant difference in the depth and width of grooves in either Si<sub>3</sub>N<sub>4</sub> or SiC. When the material is irradiated at the same scan duration, average power density and total energy density are constant in spite of different scan speed. The relation between total energy density and average power density is as follows:

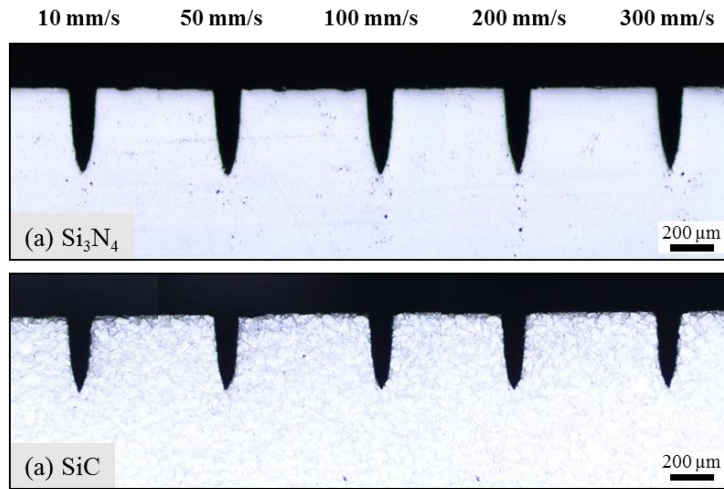
$$E_{total} = E_{1scan} \times N$$

$$E_{total} = P_a \times t$$

$$E_{total} = P_a \times \frac{L}{v} \times N$$



**Figure 4. 14 The relation between dimensions of channel and flow rate of water when machining silicon compound ceramics by laser beam in water: (a)  $\text{Si}_3\text{N}_4$ , (b)  $\text{SiC}$ .**

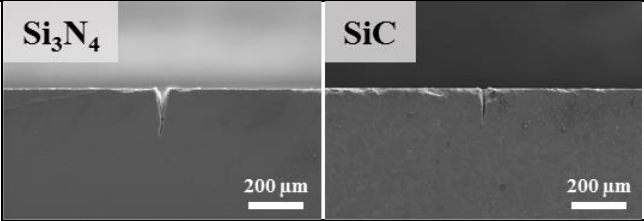
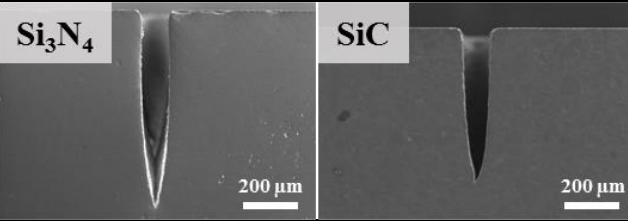


**Fig. 4.15 Cross section views of micro-channels obtained by hydrothermal reactive laser beam machining with different scan speed: (a)  $\text{Si}_3\text{N}_4$ , (b)  $\text{SiC}$ .**

$E_{total}$ ,  $E_{1scan}$ ,  $P_a$ ,  $N$ ,  $t$ ,  $L$ , and  $v$  are the total energy density, the energy density per single scan, the average power density, the scan repeat count, the scan duration, the length of scan path, and the scan speed. Increased scan speed at the same scan duration decreases an energy density per single scan. However, an average power density is constant, because a scan repeat count increases to maintain a constant scan duration. Consequently, a total energy density is constant because of the same average power density and scan duration. Therefore, the dimensions of the machined grooves are not influenced by the scan speed at the same scan duration.

The effect of laser condition on the LBM of silicon compound ceramics is summarized in Table 4.1. Compared to grooves machined in air, the deeper groove was able to be machined in water under the same machining conditions. By increasing laser power, the depth and width of grooves were able to be increased, but an increasing rate of the depth and width were larger in water compared with the air due to the hydrothermal reaction. Also, the depth of grooves was able to be increased in water by increasing scan repeat count, while the depth was converged in air despite the increasing scan repeat count. As a result, by increasing the scan repeat count, high aspect ratio grooves were able to be machined in  $\text{Si}_3\text{N}_4$  and  $\text{SiC}$  using hydrothermal reactive LBM.

**Table 4.1 Summary of the effects of laser conditions on the grooves machined in air and water.**

Process	LBM in air	LBM in water
Shape of groove		
	Laser power: 6 W (Si <sub>3</sub> N <sub>4</sub> ) 8 W (SiC), Scan repeat count: 20000, Scan speed: 100 mm/s	
Laser power	<ul style="list-style-type: none"> <li>● High laser power</li> <li>→ Increase of depth &amp; width</li> <li>● Small increasing rate of MRR</li> </ul>	<ul style="list-style-type: none"> <li>● High laser power</li> <li>→ Increase of depth &amp; width</li> <li>● Large increasing rate of MRR</li> </ul>
Scan repeat count	<ul style="list-style-type: none"> <li>● High scan repeat count</li> <li>→ Conversion of depth</li> <li>→ Conversion of width</li> </ul>	<ul style="list-style-type: none"> <li>● High scan repeat count</li> <li>→ Conversion of depth</li> <li>→ Conversion of width</li> </ul>
Scan speed	<ul style="list-style-type: none"> <li>● Negligible effect</li> </ul>	<ul style="list-style-type: none"> <li>● Negligible effect</li> </ul>



# Chapter 5

## Fabrication of various micro structure

In this chapter, various shaped micro-structures were fabricated in silicon compound ceramics using hydrothermal reactive LBM. To demonstrate various structuring is possible using hydrothermal reactive LBM, micro-channel and micro-pin arrays were fabricated, and cutting of thin ceramic sheet was conducted. In fabrication of micro-channels, the effect of line interval on the shape of channel was investigated. Then, various shaped micro-channels were fabricated, such as straight channels, wedged channels, and waved channels. In fabrication of micro-pin arrays, the effect of line interval and scan repeat count were investigated. Finally, to compare the processability of hydrothermal reactive LBM with other micro-processes for micro-machining of silicon compound ceramics, cutting of thin ceramic sheet was conducted.

## 5.1. Micro Channel

In previous chapter, the effects of machining conditions on the machining were verified using a single scan path. However, using a single scan path is limited in fabrication of various shaped structure. Although the depth of micro-structure can be controlled using a single scan path with combining various laser conditions, the width of groove is not controlled easily. Since high laser power increase the both width and depth of structure, using a single scan path is not proper for fabrication of various shaped structure, and especially structure with wide width.

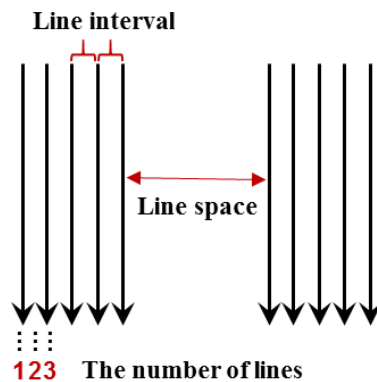


**Fig. 5.1 Multiple scan paths used in micro-channel machining.**

Therefore, multiple scan paths are used, and the effect of line interval was investigated to control the width of structure. Figure 5.1 shows multiple scan path used for micro-channel machining. By changing the line interval of multiple scan paths, the width of machined channels were be able to be controlled.

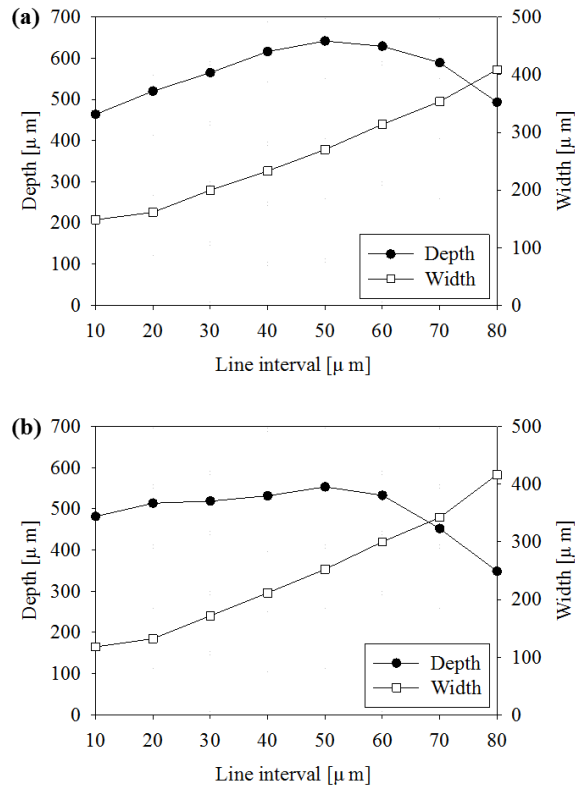


**Figure 5.2** The relation between dimensions of channel and line interval when machining silicon compound ceramics by laser beam in water: (a) Si<sub>3</sub>N<sub>4</sub>, (b) SiC.

Figure 5.2 shows the relation between the dimensions of grooves and the line interval when the Si<sub>3</sub>N<sub>4</sub> and SiC were machined in water. These structuring results of Si<sub>3</sub>N<sub>4</sub> and SiC were carried out under laser power of 6 W and 8 W, respectively, scan repeat count of 1000 times, and the number of lines of 5 lines. The width of channel entrances increased with increasing line interval in both materials.

However, the depth of micro-channel was maximum at the line space of 40 μm in both materials. When line interval is smaller than 40 μm, the flushing of water is difficult because of small entrance width of channel. Therefore, the depth of channel increased as increasing line interval, because increased flushing of water assisted the ablation of silicon compound ceramics. However, when line interval is larger than 40 μm, the depth of channel decreased as increasing line interval, because of decreased energy density. The total energy irradiated on a workpiece is as follows:

$$E_{total} = (P \times N_s \times N_{sl}) / f$$

$E_{total}$ ,  $P$ ,  $f$ ,  $N_s$ , and  $N_{sl}$  are the total energy irradiated on a workpiece, the laser power, the frequency of laser, the scan repeat count, and the number of scan paths, respectively. Increasing line interval decreases the energy density since

increasing line interval increases the irradiated area, even if the total energy is constant. As a result, the decreased energy density decreased the depth of channels. Furthermore, in case of line interval above 60  $\mu\text{m}$ , the structuring was incomplete, because overlapping between near lines was not occurred. Therefore, line interval of 40  $\mu\text{m}$  was suitable for efficient micro-channel structuring. The cross section of the micro-channels in  $\text{Si}_3\text{N}_4$  and  $\text{SiC}$  are shown in Figure 5.3 and 5.4, respectively.

Micro-channel arrays were fabricated on  $\text{Si}_3\text{N}_4$  and  $\text{SiC}$  using LBM in water to evaluate processability. Figures 5.5 shows the SEM micrographs of micro-channel arrays fabricated on  $\text{Si}_3\text{N}_4$  and  $\text{SiC}$ , respectively. The micro-channels were machined using a multiple scan path with line intervals of 40  $\mu\text{m}$ . On  $\text{Si}_3\text{N}_4$  and  $\text{SiC}$ , each straight channel with a 690  $\mu\text{m}$  and a 500  $\mu\text{m}$  depth were fabricated. The width and pitch of both channels were 210  $\mu\text{m}$  and 100  $\mu\text{m}$ , respectively. Micro-channels with various shape also textured additionally. Figure 5.6 and 5.7 show the resulted wedged channel arrays and waved channel arrays by using different laser scan paths. As a result, we could achieve a structuring of silicon compound ceramics with various shape.

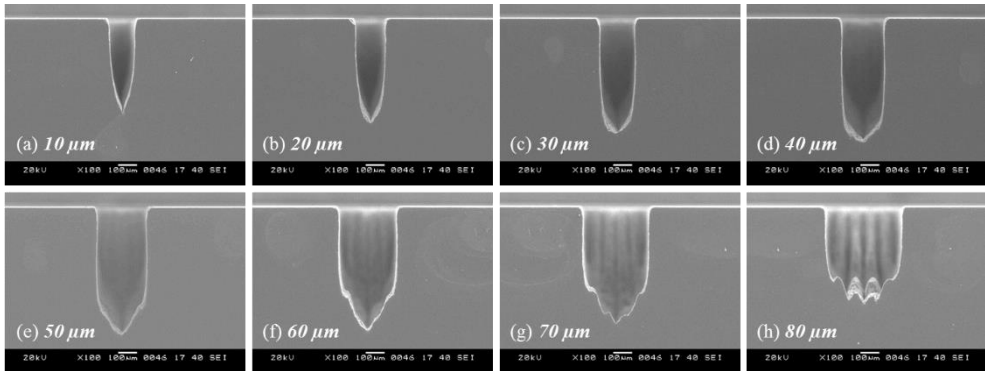


**Fig. 5.3** Cross section views of micro-channels in  $\text{Si}_3\text{N}_4$  obtained by hydrothermal reactive laser beam machining with different line interval: (a)  $10\ \mu\text{m}$ ; (b)  $20\ \mu\text{m}$ ; (c)  $30\ \mu\text{m}$ ; (d)  $40\ \mu\text{m}$ ; (e)  $50\ \mu\text{m}$ ; (f)  $60\ \mu\text{m}$ ; (g)  $70\ \mu\text{m}$ ; (h)  $80\ \mu\text{m}$ .

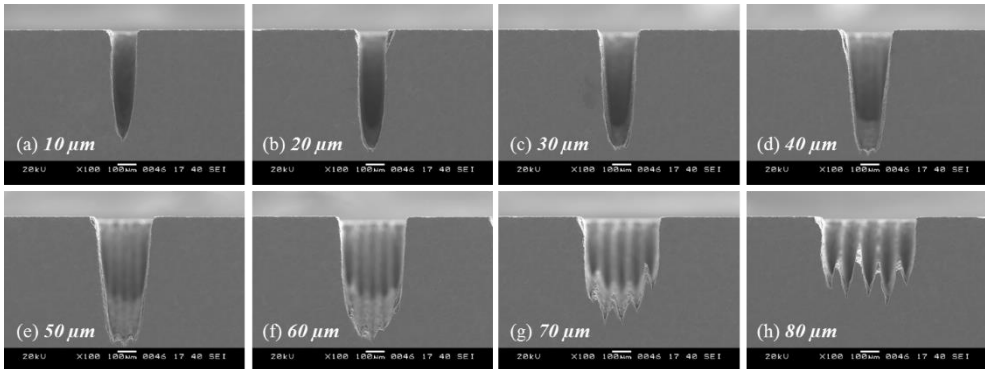


**Fig. 5.4** Cross section views of micro-channels in  $\text{SiC}$  obtained by hydrothermal reactive laser beam machining with different line interval: (a)  $10\ \mu\text{m}$ ; (b)  $20\ \mu\text{m}$ ; (c)  $30\ \mu\text{m}$ ; (d)  $40\ \mu\text{m}$ ; (e)  $50\ \mu\text{m}$ ; (f)  $60\ \mu\text{m}$ ; (g)  $70\ \mu\text{m}$ ; (h)  $80\ \mu\text{m}$ .

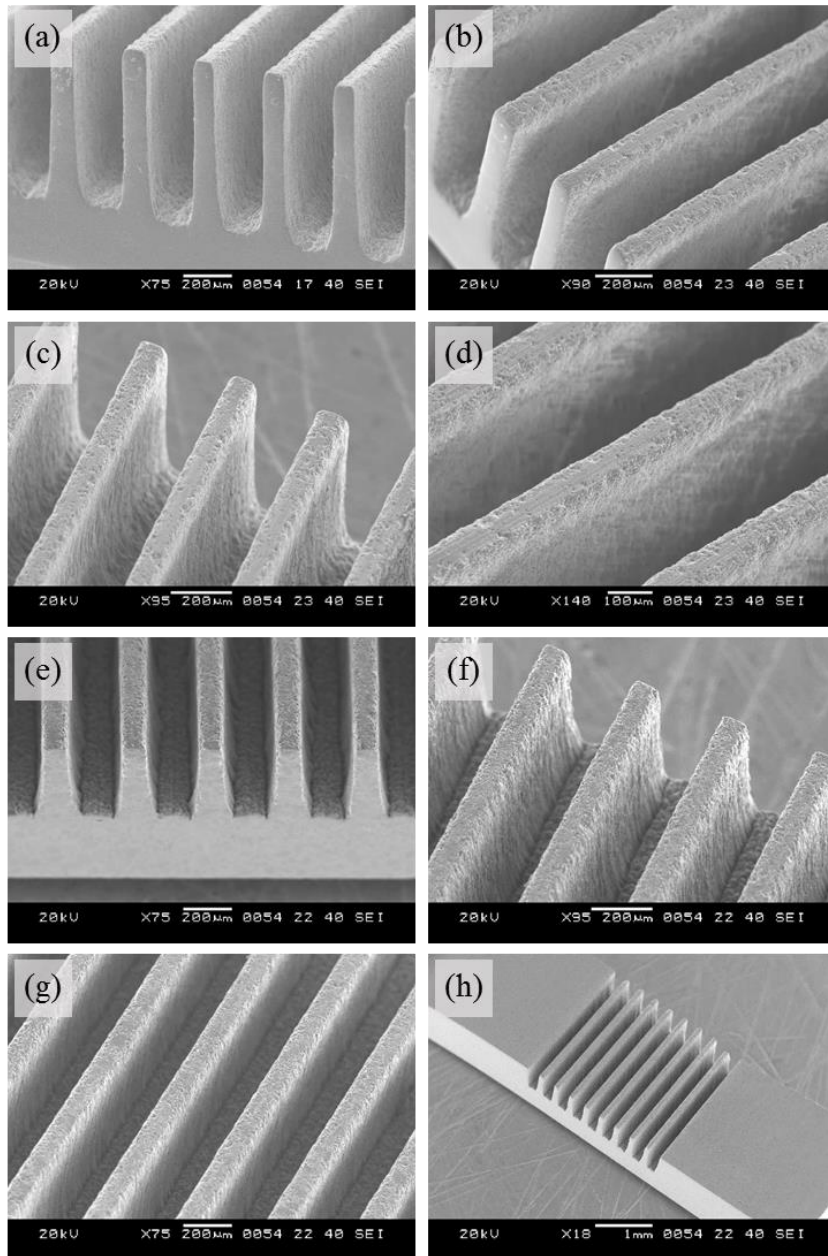


**Fig. 5.5 SEM micrographs of micro-channel arrays using hydrothermal reactive laser beam machining using multiple scan path: (a-d) in  $\text{Si}_3\text{N}_4$ , (e-h) in  $\text{SiC}$ .**

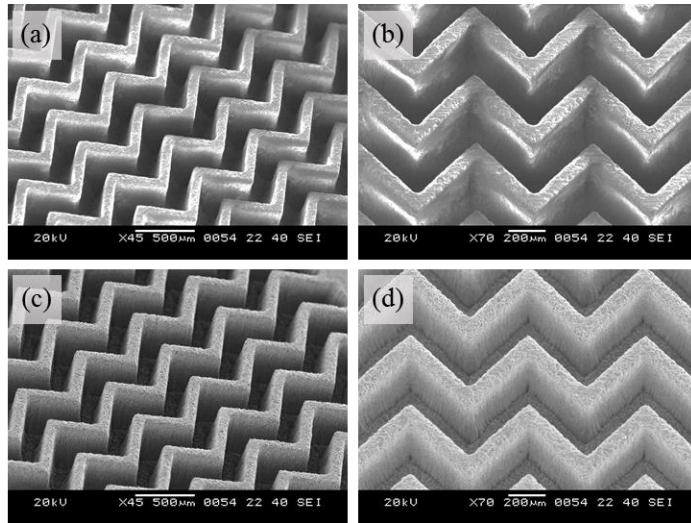


**Fig. 5.6 SEM micrographs of wedged micro-channel arrays using hydrothermal reactive laser beam machining: (a, b) in  $\text{Si}_3\text{N}_4$ , (c, d) in  $\text{SiC}$**

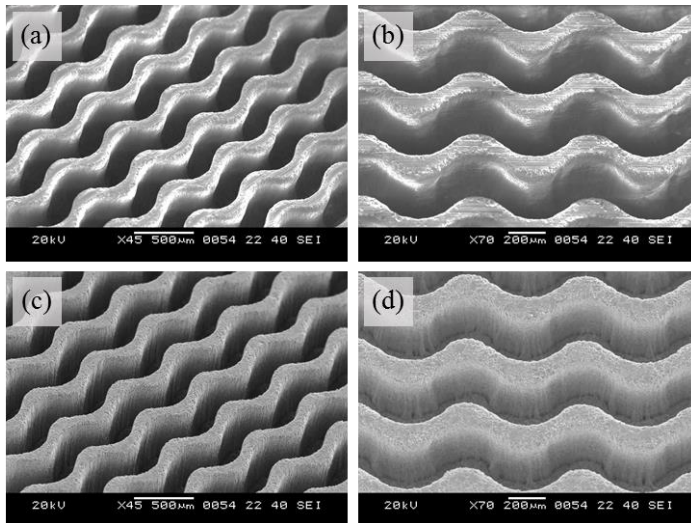


**Fig. 5.7 SEM micrographs of waved micro-channel arrays using hydrothermal reactive laser beam machining: (a, b) in  $\text{Si}_3\text{N}_4$ , (c, d) in  $\text{SiC}$**



## 5.2. Micro Pin

Micro-pin arrays were fabricated on  $\text{Si}_3\text{N}_4$  and SiC using hydrothermal reactive LBM to evaluate processability. Also, micro-pin arrays processed in water were compared with micro-pin arrays process in air. Figure 5.8 shows micro-pin arrays machined in water and air. When the micro-pin-array was processed by hydrothermal reactive LBM, a single laser scan path is suitable, because of high material removal rate. However, since the material removal rate of LBM in air is insufficient to machine micro-pin arrays, micro-pin arrays were not able to be machined in air by using a single laser scan path. Therefore, to compare the process under each optimal machining conditions, multiple laser scan paths with high laser intensity were applied during LBM in air to increase material removal rate for suitable micro-pin fabrication. The laser scan paths used in machining of micro-pin arrays were shown in Figure 5.9. The effects of line space and scan repeat count on the machining were investigated during LBM in air and water.

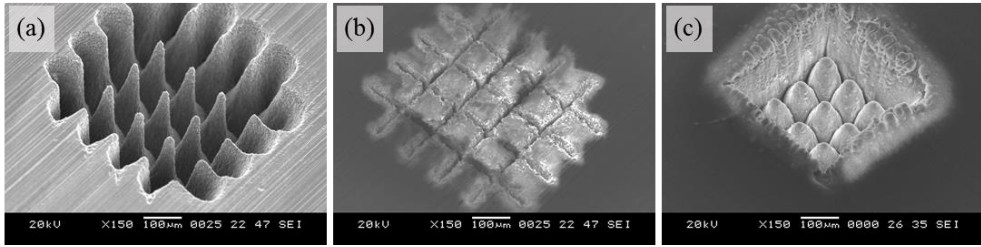


**Fig. 5.8 SEM micrographs of micro-pin arrays machined in  $\text{Si}_3\text{N}_4$ : (a) using a single laser scan path by LBM in water; (b) using a single laser scan path by LBM in air; (c) using multiple scan paths by LBM in air.**

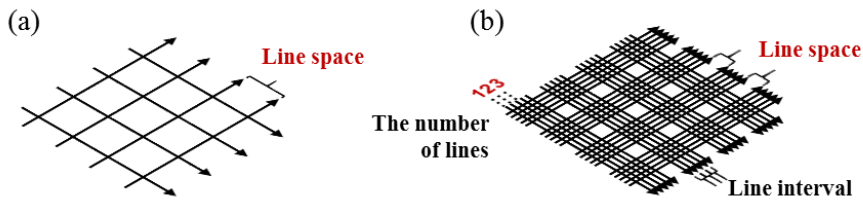


**Fig. 5.9 Laser scan path used to fabricate micro-pin arrays: (a) a single laser scan path, (b) multiple laser scan path.**

Figure 5.10 and 5.11 show SEM micrographs of micro-pin arrays with different line space during hydrothermal reactive LBM of  $\text{Si}_3\text{N}_4$  and  $\text{SiC}$ , respectively. The structuring results of  $\text{Si}_3\text{N}_4$  were carried out under laser power of 4 W, scan repeat count of 5000 times, and scan speed of 100 mm/s. The structuring results of  $\text{SiC}$  were carried out under laser power of 5 W, scan repeat count of 3000 times, and scan speed of 100 mm/s. The tip radius of

micro-pins in Si<sub>3</sub>N<sub>4</sub> and SiC was reduced as decreasing line space. However, when line space was smaller than 100 μm, the formation of micro-pins was irregular. The micro-pins with line space smaller than 100 μm were easily broken because of excessive small tip radius. Therefore, the line space of 100 μm was suitable to fabricate the regular micro-pin arrays with small tip radius.

Figure 5.12 and 5.13 show SEM micrographs of micro-pin arrays with different scan repeat count during hydrothermal reactive LBM of Si<sub>3</sub>N<sub>4</sub> and SiC, respectively. The structuring results of Si<sub>3</sub>N<sub>4</sub> and SiC were carried out under laser power of 4 W and 5 W, respectively. Also, the scan speed of 100 mm/s, and the line interval of 100 μm were used for the experiments. As the scan repeat count increased, vertical length of pins increased and tip radius of pins decreased. However, the vertical length and tip radius of pins were converged over scan repeat count of 5000 times and 3000 times, in case of Si<sub>3</sub>N<sub>4</sub> and SiC, respectively. Therefore, the scan repeat count of 5000 times and 3000 times were selected as effective machining conditions for micro-pin arrays fabrication.

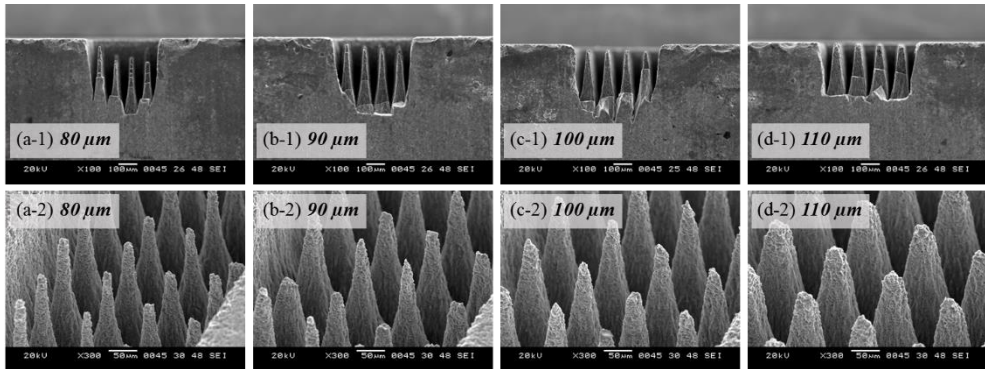


**Fig. 5.10** Cross section views and tilted views of micro-pin arrays in Si<sub>3</sub>N<sub>4</sub> obtained by hydrothermal reactive laser beam machining with different line space: (a) 80 μm; (b) 90 μm; (c) 100 μm; (d) 110 μm.

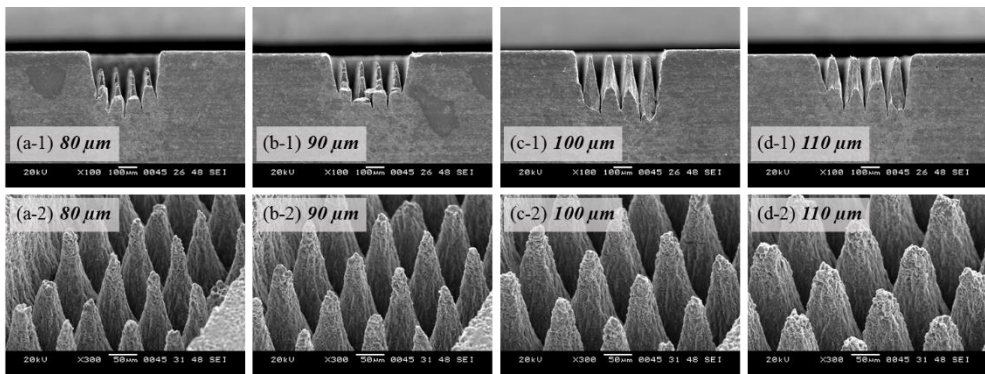


**Fig. 5.11** Cross section views and tilted views of micro-pin arrays in SiC obtained by hydrothermal reactive laser beam machining with different line space: (a) 80 μm; (b) 90 μm; (c) 100 μm; (d) 110 μm.

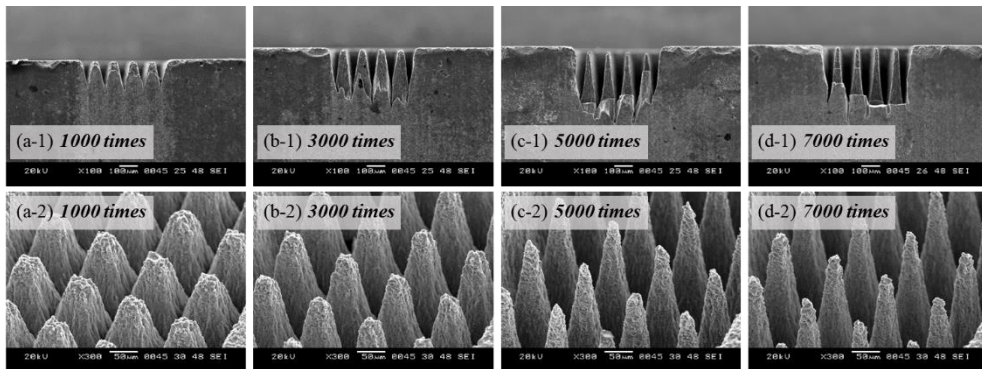


**Fig. 5.12** Cross section views and tilted views of micro-pin arrays in  $\text{Si}_3\text{N}_4$  obtained by hydrothermal reactive laser beam machining with different scan repeat count: (a) 1000 times; (b) 3000 times; (c) 5000 times; (d) 7000 times.

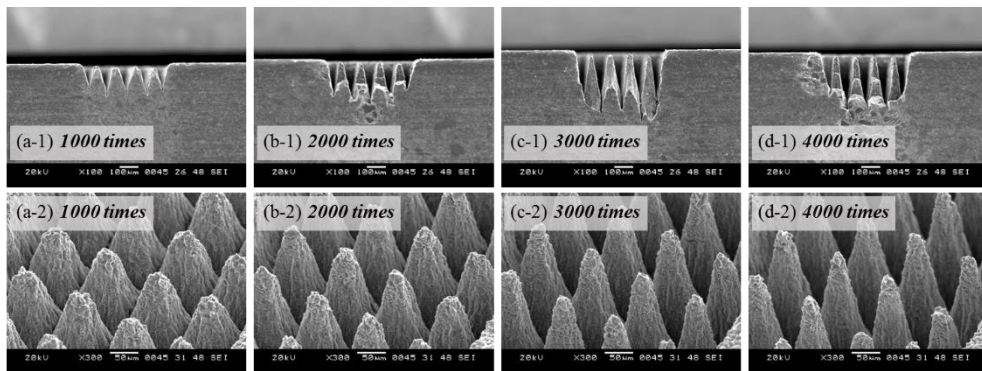


**Fig. 5.13** Cross section views and tilted views of micro-pin arrays in  $\text{SiC}$  obtained by hydrothermal reactive laser beam machining with different scan repeat count: (a) 1000 times; (b) 2000 times; (c) 3000 times; (d) 4000 times.

In case of LBM in air, likewise with the hydrothermal reactive LBM, too small line space made pin arrays irregular while too large line space made tip radius of pin arrays large. Also, increased scan repeat count increased vertical length of pins, while too many scan repeat counts made micro-pin arrays incomplete because of the formation of excessive  $\text{SiO}_2$  layer. As a result, in case of  $\text{Si}_3\text{N}_4$ , the micro-pin arrays fabrication using LBM in air was conducted with the line space of  $60\ \mu\text{m}$  and the scan repeat count of 10 times. In case of  $\text{SiC}$ , the line space of  $50\ \mu\text{m}$  and the scan repeat count of 10 times were selected for machining conditions during LBM in air. The fabricated pin arrays of  $\text{Si}_3\text{N}_4$  with different line space and scan repeat count during LBM in air are shown in Figure 5.14 and 5.15, respectively. Also, the fabricated pin arrays of  $\text{SiC}$  with different line space and scan repeat count during LBM in air are shown in Figure 5.16 and 5.17, respectively.

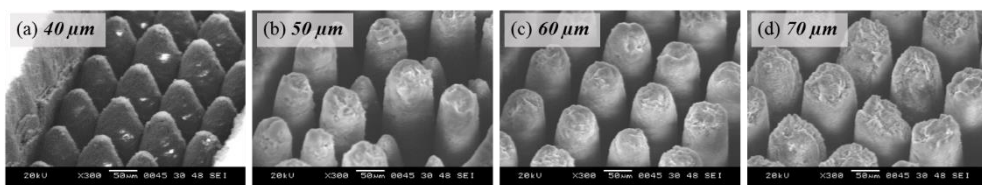


**Fig. 5.14 Tilted views of micro-pin arrays in  $\text{Si}_3\text{N}_4$  obtained by laser beam machining with different line space: (a)  $40\ \mu\text{m}$ ; (b)  $50\ \mu\text{m}$ ; (c)  $60\ \mu\text{m}$ ; (d)  $70\ \mu\text{m}$ .**

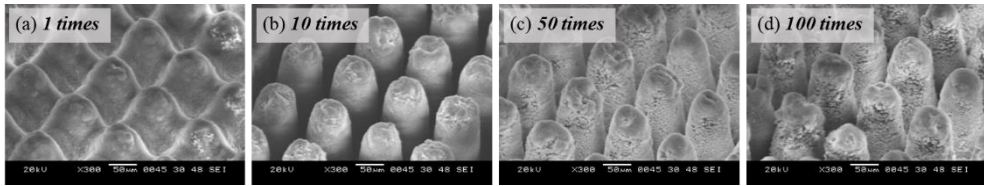


**Fig. 5.15** Tilted views of micro-pin arrays in  $\text{Si}_3\text{N}_4$  obtained by laser beam machining with different repeat count: (a) 1 times; (b) 10 times; (c) 50 times; (d) 100 times.

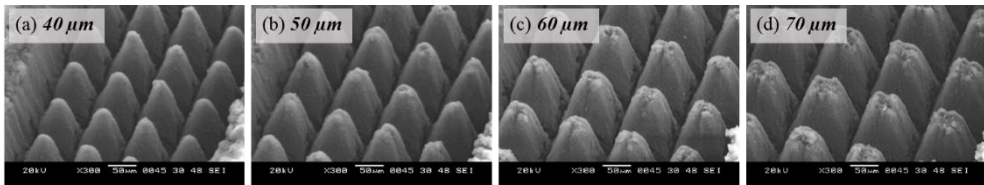


**Fig. 5.16** Tilted views of micro-pin arrays in  $\text{SiC}$  obtained by hydrothermal reactive laser beam machining with different line space: (a)  $40\ \mu\text{m}$ ; (b)  $50\ \mu\text{m}$ ; (c)  $60\ \mu\text{m}$ ; (d)  $70\ \mu\text{m}$ .

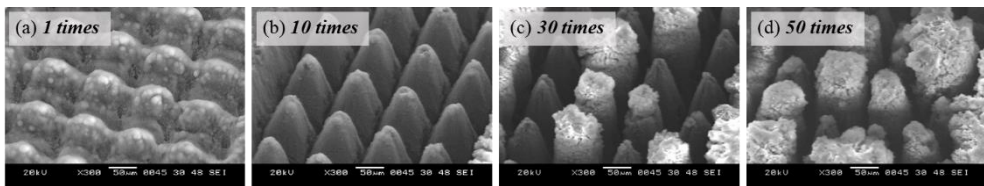


**Fig. 5.17** Tilted views of micro-pin arrays in  $\text{SiC}$  obtained by laser beam machining with different repeat count: (a) 1 times; (b) 10 times; (c) 30 times; (d) 50 times.

The micro-pin arrays of silicon compound ceramics fabricated by LBM in water and air are compared in Figure 5.18. Compared to pin-arrays fabricated in air, the longer vertical length and smaller tip radius of pins were able to be achieved in water under each optimum machining conditions. When fabricating micro-pin arrays using LBM in air, SiO<sub>2</sub> generated by laser ablation of silicon compound ceramics covered pin structure and reduced tip radius. However, by using hydrothermal reactive LBM, the micro-pin arrays with high quality were able to be fabricated at silicon compound ceramics, because SiO<sub>2</sub> was removed by hydrothermal reaction.



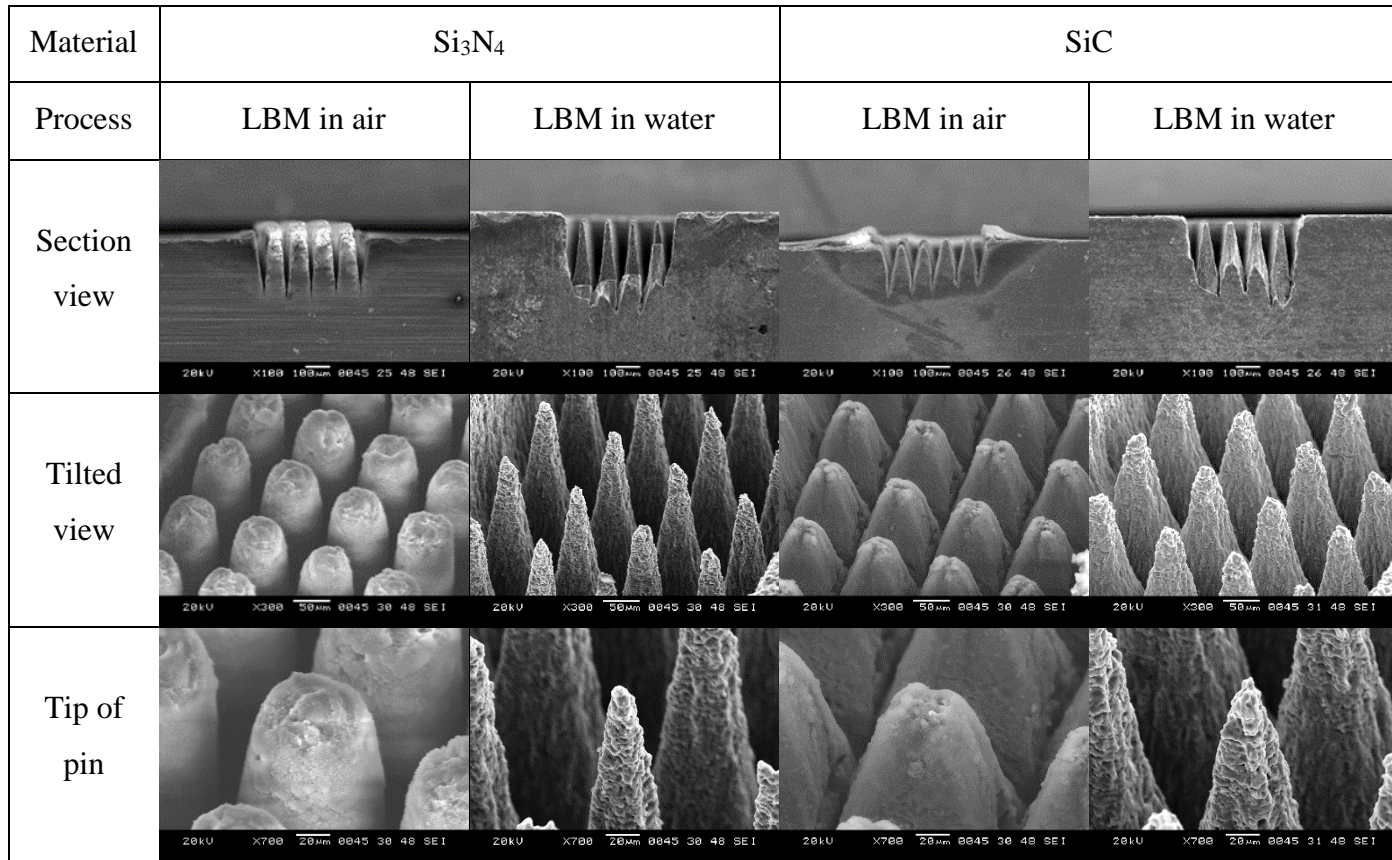


**Fig. 5.18 Comparison of the micro-pin array fabricated by laser beam machining in air and water.**

### 5.3. Cutting

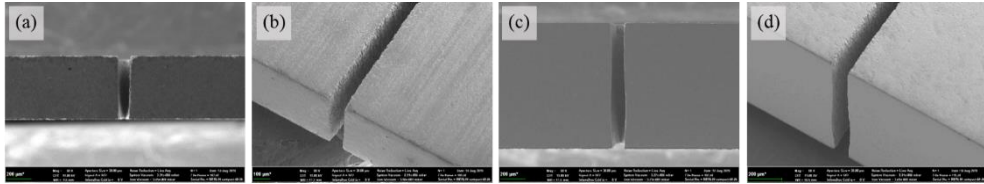
Silicon compound ceramics sheets were cut using hydrothermal reactive LBM to evaluate processability. Figures 5.19 and 5.20 show the cross section views and tilted views of cut  $\text{Si}_3\text{N}_4$  and  $\text{SiC}$  sheet, respectively. The sheets with a thickness of 0.5 mm and 1 mm were cut using hydrothermal reactive LBM with a single scan path. Cutting conditions used in the experiments and dimensions of cutting profiles are shown in Table 5.1. The  $\text{Si}_3\text{N}_4$  and  $\text{SiC}$  sheets with a thickness of 0.5 mm were able to be cut with few difference between the entrance width and the exit width. However, when  $\text{Si}_3\text{N}_4$  and  $\text{SiC}$  sheets with a thickness of 1 mm were cut, the middle of cutting plane was convex due to the multiple internal reflection of laser beam. Various shaped cutting of silicon compound sheets with a thickness of 0.5 mm also was conducted additionally. Figure 5.21 shows the resulted  $\text{Si}_3\text{N}_4$  and  $\text{SiC}$  sheets using different laser scan paths. As a result, various shaped cutting of silicon compound ceramics was able to be achieved using hydrothermal reactive LBM.

In Table 5.2, the cutting of silicon compound ceramics using hydrothermal reactive LBM are compared with other processes such as femtosecond pulsed laser beam machining, and focused ion-beam machining. Compared with

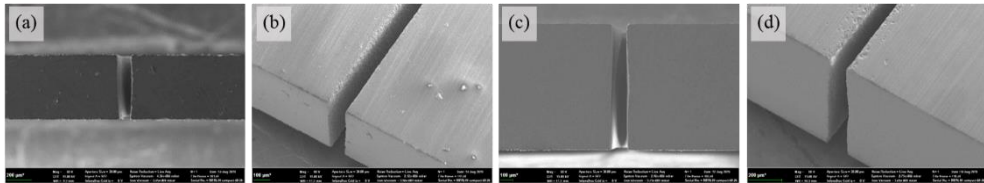
other processes, hydrothermal reactive LBM can cut silicon compound ceramics sheets with high material removal rate. However, hydrothermal reactive LBM has a limitation in minimum feature size compared with femtosecond pulsed LBM and focused ion-beam machining. Nevertheless, hydrothermal reactive LBM has an advantage in machining micrometer scale structures because of its high material removal rate and low cost for investment.

**Table 5.1 Machining conditions and resulted dimension in cutting of Si<sub>3</sub>N<sub>4</sub> and SiC sheets with a thickness of 0.5 mm and 1 mm.**

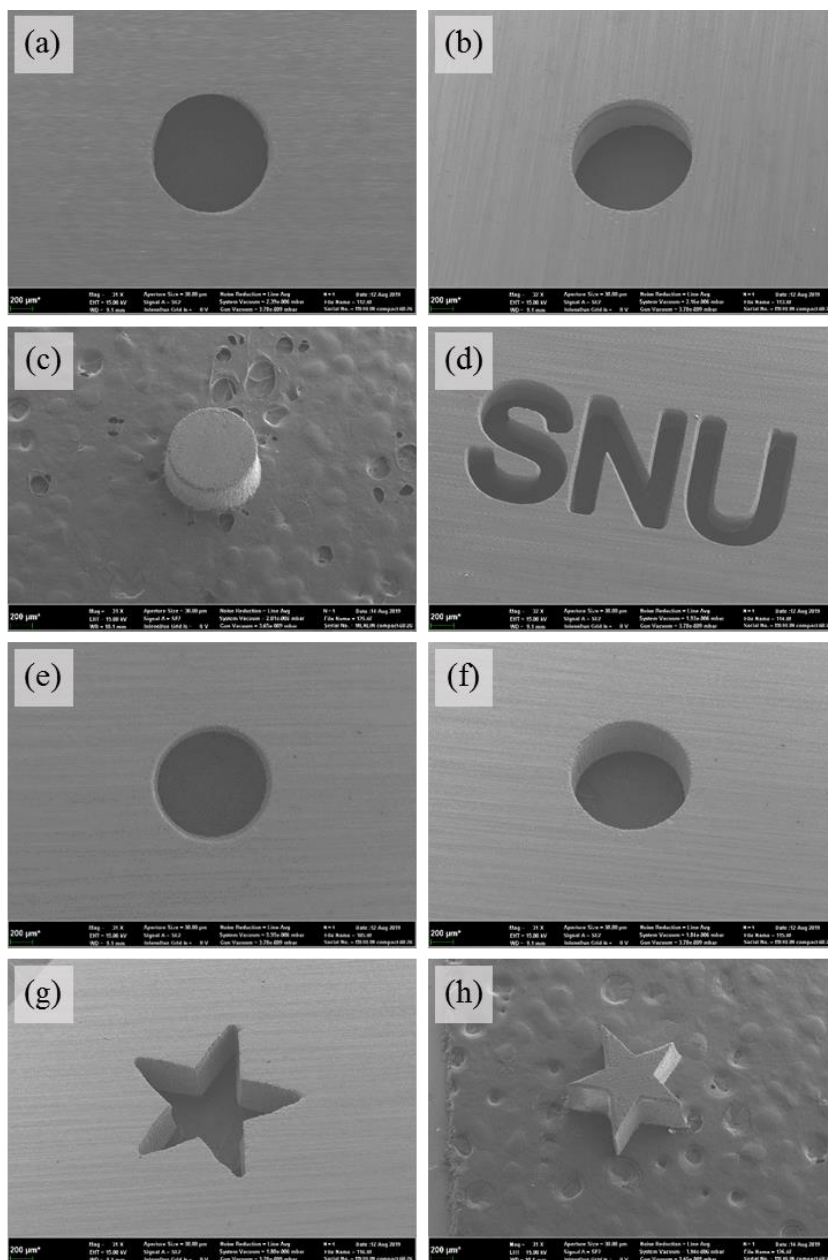
Material	Si <sub>3</sub> N <sub>4</sub>		SiC	
	0.5 mm	1 mm	0.5 mm	1 mm
Thickness	0.5 mm	1 mm	0.5 mm	1 mm
Laser power	6 W	6 W	8 W	8 W
Scan repeat count	15000	30000	20000	40000
Entrance width	115 μm	120 μm	102 μm	102 μm
Exit width	97 μm	130 μm	83 μm	103 μm



**Fig. 5.19** Cross section views and tilted views of Si<sub>3</sub>N<sub>4</sub> sheet cut by hydrothermal reactive laser beam machining: (a, b) thickness of 0.5 mm; (c, d) thickness of 1 mm.

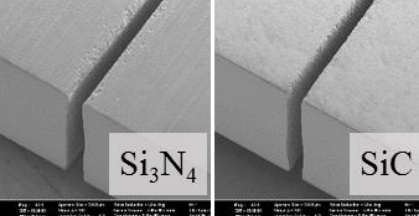
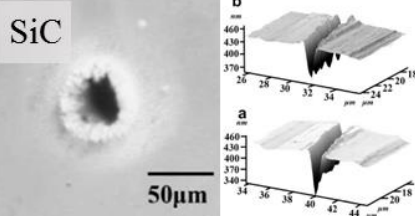
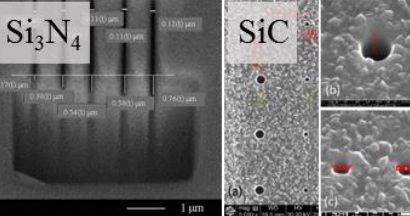


**Fig. 5.20** Cross section views and tilted views of SiC sheet cut by hydrothermal reactive laser beam machining: (a, b) thickness of 0.5 mm; (c, d) thickness of 1 mm.



**Fig. 5.21 SEM micrographs of silicon compound ceramics sheets cut by hydrothermal reactive laser beam machining using various scan path: (a-d) in  $\text{Si}_3\text{N}_4$ , (e-h) in  $\text{SiC}$ .**

**Table 5.2 Comparison of hydrothermal reactive LBM of silicon compound ceramics with other processes [53–56].**

Process	Hydrothermal reactive LBM	Femtosecond pulsed LBM	Focus Ion Beam machining
Figure			
Thickness	<ul style="list-style-type: none"> <li>● 1 mm</li> </ul>	<ul style="list-style-type: none"> <li>● 250 μm</li> </ul>	<ul style="list-style-type: none"> <li>● Si<sub>3</sub>N<sub>4</sub>: 0.54 μm</li> <li>● SiC: 200,000 μm<sup>3</sup>/s</li> </ul>
Material removal rate	<ul style="list-style-type: none"> <li>● Si<sub>3</sub>N<sub>4</sub>: 215,000 μm<sup>3</sup>/s</li> <li>● SiC: 200,000 μm<sup>3</sup>/s</li> </ul>	<ul style="list-style-type: none"> <li>● SiC: 4.02 μm<sup>3</sup>/s</li> </ul>	<ul style="list-style-type: none"> <li>● Si<sub>3</sub>N<sub>4</sub>: 2.42 × 10<sup>-3</sup> μm<sup>3</sup>/s</li> <li>● SiC: 3.18 × 10<sup>-5</sup> μm<sup>3</sup>/s</li> </ul>
Maximum aspect ratio	<ul style="list-style-type: none"> <li>● 9 – 11</li> </ul>	<ul style="list-style-type: none"> <li>● 6 – 10</li> </ul>	<ul style="list-style-type: none"> <li>● 5 – 10</li> </ul>
Minimum feature size	<ul style="list-style-type: none"> <li>● 90 – 110 μm</li> </ul>	<ul style="list-style-type: none"> <li>● SiC: 40 μm</li> </ul>	<ul style="list-style-type: none"> <li>● 100 – 110 μm</li> </ul>
Cost/ Maintenance	<ul style="list-style-type: none"> <li>● Nanosecond pulsed laser</li> <li>● Widespread use in industry</li> </ul>	<ul style="list-style-type: none"> <li>● Costly investment</li> </ul>	<ul style="list-style-type: none"> <li>● Costly investment</li> <li>● Need of vacuum chamber</li> </ul>

# Chapter 6

## Conclusion

The micro-structuring of silicon compound ceramics was carried out using hydrothermal reactive LBM. With an assist of hydrothermal reaction of silicon compound ceramics, machining efficiency of LBM was improved in water. Ablation behavior and machining principle of underwater LBM of silicon compound ceramics were investigated. Water increased the ablated volume as the laser beam irradiation was repeated, while the ablated volume converged in air due to the accumulation of a recast layer. The recast layer composed of silicon dioxide did not form when the materials were machined in water. Consequently, the chemical composition was not changed by LBM in water. To verify the reason that the oxide layer did not form in water, laser irradiation and chemical composition analysis of the machined surface were conducted in water and kerosene. In water the oxide layer was removed by laser irradiation, whereas the oxide layer was not eliminated in kerosene. As a result, it was confirmed that a hydrothermal reaction assisted in the removal

of an oxide layer and enabled the silicon compound ceramics to be machined continuously in water.

Then, the effect of machining parameters including the flow rate of water, laser power, scan repeat count, and scan speed were investigated. As the flow rate of water increased, a deeper and narrower groove was able to be machined. Also, as the laser power and the scan repeat count increased, a deeper groove was able to be machined in water, while it was difficult to increase the depth of the groove in air. The scan speed did not influence the dimensions of the machined grooves at the equal scan duration. As a result, by increasing the scan repeat count, high aspect ratio grooves were able to be machined in  $\text{Si}_3\text{N}_4$  and  $\text{SiC}$  using hydrothermal reactive LBM. Also, compared to grooves machined in air, the deeper groove was able to be machined in water under the same machining conditions.

Finally, the availability of fabricating various shaped micro-structures was identified in the LBM of silicon compound ceramics in water. Various structuring such as various shaped micro-channel array, micro-pin arrays, and cutting of thin sheets were conducted on silicon compound ceramics. The results show that for the micro-structuring of silicon compound ceramics,



hydrothermal reactive LBM is an effective process in aspects of quality and efficiency.

In future, more researches are needed to make functional surface on the silicon compound ceramics by micro-structuring using hydrothermal reactive LBM. In addition, feasibility for effectiveness of hydrothermal reactive LBM using other laser source such as femtosecond laser should be considered in a future work.

# Reference

- [1] Samant AN, Dahotre NB. Laser Machining of Structural Ceramics-A Review. *J Eur Ceram Soc* 2009;29:969–93.  
doi:10.1016/j.jeurceramsoc.2008.11.010 %/ ELSEVIER SCI LTD.
- [2] Kirchner HP. Damage Penetration at Elongated Machining Grooves in Hot-Pressed Si<sub>3</sub>N<sub>4</sub>. *J Am Ceram Soc* 1984;67:127–32.  
doi:10.1111/j.1151-2916.1984.tb09629.x.
- [3] Zhang B, Zheng XL, Tokura H, Yoshikawa M. Grinding induced damage in ceramics. *J Mater Process Technol* 2003;132:353–64.  
doi:10.1016/S0924-0136(02)00952-4.
- [4] Thoe TB, Aspinwall DK, Wise MLH. Review on ultrasonic machining. *Int J Mach Tools Manuf* 1998;38:239–55.  
doi:10.1016/S0890-6955(97)00036-9.
- [5] Srinivasu DS, Axinte DA, Shipway PH, Folkes J. Influence of kinematic operating parameters on kerf geometry in abrasive waterjet machining of silicon carbide ceramics. *Int J Mach Tools Manuf* 2009;49:1077–88. doi:10.1016/j.ijmachtools.2009.07.007.

- [6] Abdo BMA, Anwar S, El-Tamimi A. Machinability study of bioactive ceramic by milling microchannels using rotary ultrasonic machining. *J Manuf Process* 2019;43:175–91. doi:10.1016/j.jmapro.2019.05.031.
- [7] Schubert A, Zeidler H, Oschätzchen MH, Schneider J, Hahn M. cing Micro-EDM using Ultrasonic Vibration and Approaches for Machining of Nonconducting Ceramics. *Strojniški Vestn – J Mech Eng* 2013;59:156–64. doi:10.5545/sv-jme.2012.442.
- [8] Banu A, Ali MY, Rahman MA. Micro-electro discharge machining of non-conductive zirconia ceramic: investigation of MRR and recast layer hardness. *Int J Adv Manuf Technol* 2014;75:257–67. doi:10.1007/s00170-014-6124-9.
- [9] Schubert A, Zeidler H, Kühn R, Hackert-Oschätzchen M. Microelectrical Discharge Machining: A Suitable Process for Machining Ceramics. *J Ceram* 2015;2015:1–9. doi:10.1155/2015/470801.
- [10] Muttamara A, Fukuzawa Y, Mohri N, Tani T. Probability of precision micro-machining of insulating Si<sub>3</sub>N<sub>4</sub> ceramics by EDM. *J Mater Process Technol* 2003;140:243–7. doi:10.1016/S0924-

0136(03)00745-3.

- [11] Muttamara A, Janmanee P, Fukuzawa Y. A Study of Micro-EDM on Silicon Nitride Using Electrode Materials. *Int Trans J Eng* 2010;1:1906–9642.
- [12] Zeller F, Hösel T, Müller C, Reinecke H. Microstructuring of non-conductive silicon carbide by electrical discharge machining. *Microsyst Technol* 2014;20:1875–80. doi:10.1007/s00542-013-1965-y.
- [13] Pham DT, Dimov SS, Petkov P V. Laser milling of ceramic components. *Int J Mach Tools Manuf* 2007;47:618–26. doi:10.1016/j.ijmachtools.2006.05.002.
- [14] Wang H, Lin H, Wang C, Zheng L, Hu X. Laser drilling of structural ceramics—A review. *J Eur Ceram Soc* 2017;37:1157–73. doi:10.1016/j.jeurceramsoc.2016.10.031.
- [15] Mohammed MK, Umer U, Al-Ahmari A. Optimization of Nd:YAG laser for microchannels fabrication in alumina ceramic. *J Manuf Process* 2019;41:148–58. doi:10.1016/j.jmapro.2019.03.036.
- [16] Wang X, Huang Y, Xing Y, Fu X, Zhang Z, Ma C. Fabrication of

- micro-channels on Al<sub>2</sub>O<sub>3</sub>/TiC ceramics using picosecond laser induced plasma micromachining. *J Manuf Process* 2019;44:102–12. doi:10.1016/j.jmapro.2019.05.048.
- [17] Shigematsu I, Kanayama K, Tsuge A, Nakamura M. Analysis of constituents generated with laser machining of Si<sub>3</sub>N<sub>4</sub> and SiC. *J Mater Sci Lett* 1998;17:737–9. doi:10.1023/A:1006606810476.
- [18] Meiners E, Wiedmaier M, Dausinger F, Krastel K, Masek I, Kessler A. Micro machining of ceramics by pulsed Nd:YAG laser. *Int Congr Appl Lasers Electro-Optics* 2018;327:327–36. doi:10.2351/1.5058456.
- [19] Islam MU, Campbell G. Laser Machining of Ceramics: A Review. *Mater Manuf Process* 1993;8:611–30. doi:10.1080/10426919308934870.
- [20] Tshabalala LC, Pityana S. Surface texturing of Si<sub>3</sub>N<sub>4</sub>-SiC ceramic tool components by pulsed laser machining. *Surf Coatings Technol* 2016;289:52–60. doi:10.1016/j.surfcoat.2016.01.028.
- [21] Kurita T, Komatsuzaki K, Hattori M. Advanced material processing with nano- and femto-second pulsed laser. *Int J Mach Tools Manuf* 2008;48:220–7. doi:10.1016/j.ijmachtools.2007.08.012.

- [22] Ahmed N, Darwish S, Alahmari AM. Laser Ablation and Laser-Hybrid Ablation Processes: A Review. *Mater Manuf Process* 2016;31:1121–42. doi:10.1080/10426914.2015.1048359.
- [23] Kruusing A. Underwater and water-assisted laser processing: Part 2 - Etching, cutting and rarely used methods. *Opt Lasers Eng* 2004;41:329–52. doi:10.1016/S0143-8166(02)00143-4.
- [24] Morita N, Ishida S, Fujimori Y, Ishikawa K. Pulsed laser processing of ceramics in water. *Appl Phys Lett* 1988;52:1965–6. doi:10.1063/1.99591.
- [25] Dolgaev SI, Lyalin AA, Shafeev GA, Voronov V V. Fast etching and metallization of SiC ceramics with copper-vapor-laser radiation. *Appl Phys A Mater Sci Process* 1996;63:75–9. doi:10.1007/BF01579748.
- [26] Geiger M, Becker W, Rebhan T, Hutfless J, Lutz N. Increase of efficiency for the XeCl excimer laser ablation of ceramics. *Appl Surf Sci* 1996;96–98:309–15. doi:10.1016/0169-4332(95)00435-1.
- [27] Wee LM, Khoong LE, Tan CW, Lim GC. Solvent-assisted laser drilling of silicon carbide. *Int J Appl Ceram Technol* 2011;8:1263–76. doi:10.1111/j.1744-7402.2010.02575.x.

- [28] Geiger M, Roth S, Becker W. Microstructuring and surface modification by excimer laser machining under thin liquid films. *ALT'97 Int Conf Laser Surf Process* 1998;3404:200–8. doi:10.1117/12.308616.
- [29] Brook MR, Shafeev GA. Laser-assisted engraving of HgCdTe under a liquid layer. *Appl Surf Sci* 1992;54:336–40. doi:10.1016/0169-4332(92)90066-7.
- [30] Shafeev GA, Obraztsova ED, Pimenov SM. Laser-assisted etching of diamonds in air and in liquid media. *Mater Sci Eng B* 1997;46:129–32. doi:10.1016/S0921-5107(96)01947-2.
- [31] Dolgaev SI, Voronov V V., Shafeev GA, Fauquet-Ben Ammar C, Themlin JM, Cros A, et al. Laser-induced fast etching and metallization of SiC ceramics. *Appl Surf Sci* 1997;109–110:559–62. doi:10.1016/S0169-4332(96)00634-4.
- [32] Ageev VA, Bokhonov AF, Zhukovskii V V., Yankovskii AA. Dynamics of processes occurring in laser ablation of metals in a liquid. *J Appl Spectrosc* 1997;64:683–8. doi:10.1007/bf02675334.
- [33] Sakka T, Iwanaga S, Ogata YH, Matsunawa A, Takemoto T. Laser ablation at solid-liquid interfaces: An approach from optical emission

- spectra. *J Chem Phys* 2000;112:8645–53. doi:10.1063/1.481465.
- [34] Ohara J, Nagakubo M, Kawahara N, Hattori T. High aspect ratio etching by infrared laser induced micro bubbles. *Proc IEEE Micro Electro Mech Syst* 1997:175–9.
- [35] Kruusing A, Leppävuori S, Uusimäki A, Petrêtis B, Makarova O. Micromachining of magnetic materials. *Sensors Actuators, A Phys* 1999;74:45–51. doi:10.1016/S0924-4247(98)00343-4.
- [36] Dupont A, Caminat P, Bournot P, Gauchon JP. Enhancement of material ablation using 248, 308, 532, 1064 nm laser pulse with a water film on the treated surface. *J Appl Phys* 1995;78:2022–8. doi:10.1063/1.360178.
- [37] Zweig AD, Deutsch TF. Shock waves generated by confined XeCl excimer laser ablation of polyimide. *Appl Phys B Photophysics Laser Chem* 1992;54:76–82. doi:10.1007/BF00331737.
- [38] Yan Y, Li L, Sezer K, Wang W, Whitehead D, Ji L, et al. CO<sub>2</sub> laser underwater machining of deep cavities in alumina. *J Eur Ceram Soc* 2011;31:2793–807. doi:10.1016/j.jeurceramsoc.2011.06.015.
- [39] Zhu S, Lu YF, Hong MH, Chen XY. Laser ablation of solid



- substrates in water and ambient air. *J Appl Phys* 2001;89:2400–3.  
doi:10.1063/1.1342200.
- [40] Sato T, Murakami T, Endo T, Shimada M, Komeya K, Kameda T, et al. Corrosion of silicon nitride ceramics under hydrothermal conditions. *J Mater Sci* 1991;26:1749–54. doi:10.1007/BF00543597.
- [41] Nickel KG, Däumling U, Weisskopf K. Hydrothermal Reactions of Si<sub>3</sub>N<sub>4</sub>. *Key Eng Mater* 1993;89–91:295–300.  
doi:10.4028/www.scientific.net/KEM.89-91.295.
- [42] Kim WJ, Hwang HS, Park JY. Corrosion behavior of reaction-bonded silicon carbide ceramics in high-temperature water. *J Mater Sci Lett* 2002;21:733–5. doi:10.1023/A:1015797324658.
- [43] Oda K, Yoshio T, Miyamoto Y, Koizumi M. Hydrothermal Corrosion of Pure, Hot Isostatically Pressed Silicon Nitride. *J Am Ceram Soc* 1993;76:1365–8. doi:10.1111/j.1151-2916.1993.tb03768.x.
- [44] Somiya S. Hydrothermal corrosion of nitride and carbide of silicon. *Mater Chem Phys* 2001;67:157–64. doi:10.1016/S0254-0584(00)00434-X.
- [45] Hirayama H, Kawakubo T, Goto A, Kaneko T. Corrosion Behavior

- of Silicon Carbide in 290°C Water. *J Am Ceram Soc* 1989;72:2049–53. doi:10.1111/j.1151-2916.1989.tb06029.x.
- [46] Mullick S, Madhukar YK, Roy S, Kumar S, Shukla DK, Nath AK. Development and parametric study of a water-jet assisted underwater laser cutting process. *Int J Mach Tools Manuf* 2013;68:48–55. doi:10.1016/j.ijmactools.2013.01.005.
- [47] Grove AS. *Physics and technology of semiconductor*. 1967.
- [48] Haynes WM. *CRC Handbook of Chemistry and Physics*. 92nd ed. CRC Press: Boca Raton; 2011.
- [49] Daviau, Kierstin; Kanani, KM L. Decomposition of silicon carbide at high pressures and temperatures. *Phys Rev B* 2017;96:174102.
- [50] Huheey, J;Cottrell TL. *The strengths of chemical bonds*. 1958.
- [51] Dean JA. *Lange’s Handbook of Chemistry*. 11th ed. New York: McGraw-Hill: New York; 1979.
- [52] Lide DR. *CRC Handbook*. 84th ed. Florida: CRC Press: Boca Raton; 2003.
- [53] Li C, Shi X, Si J, Chen T, Chen F, Liang S, et al. Alcohol-assisted photoetching of silicon carbide with a femtosecond laser. *Opt*

Commun 2009;282:78–80. doi:10.1016/j.optcom.2008.09.072.

- [54] Yue S, Gu C. Nanopores fabricated by focused ion beam milling technology. 2007 7th IEEE Int Conf Nanotechnol - IEEE-NANO 2007, Proc 2007:628–31. doi:10.1109/NANO.2007.4601269.
- [55] Zamani H, Lee SW, Avishai A, Zorman CA, Sankaran RM, Feng PXL. Focused Ion-Beam (FIB) Nanomachining of Silicon Carbide (SiC) Stencil Masks for Nanoscale Patterning. Mater Sci Forum 2012;717–720:889–92. doi:10.4028/www.scientific.net/msf.717-720.889.
- [56] Kononenko T V, Konov VI, Garnov S V, Danielius R, Piskarskas A, Tamosauskas G, et al. Comparative study of the ablation of materials by femtosecond and pico- or nanosecond laser pulses. Quantum Electron 1999;29:724–8. doi:10.1070/qe1999v029n08abeh001560.

# 국문 초록

서울대학교

공과대학원

기계항공공학부

정형균

본 논문에서는 실리콘 화합물 세라믹의 수열 반응 레이저 빔 가공에 대한 연구를 진행하였다. 실리콘 화합물 세라믹은 높은 고온 강도와 내열성, 내마모성, 절연성, 내식성으로 인하여 고속 마찰 부품이나, 가스 노즐, 고성능 절삭 공구 등과 같은 다양한 분야에 적용되어 온 소재이다. 그러나 이러한 우수한 특성들은 실리콘 화합물 세라믹의 마이크로 가공을 어렵게 만들며, 산업 현장에서 실리콘 화합물 세라믹의 효율적인 사용을 제한해왔다. 세라믹 재료의 수중 레이저 빔 가공은 일반 레이저 빔 가공보다 우수한 품질

의 가공이 가능한 것으로 알려져 있다. 수중 레이저 빔 가공은 세라믹 재료 가공 시에 발생하는 재응고층과 영영향부, 크랙을 효과적으로 줄일 수 있다. 그러나 수중 가공 시 발생하는 기포와 잔여물들은 세라믹 재료의 수중 레이저 빔 가공 시 가공 효율을 감소시킨다는 한계가 있다. 또한 실리콘 화합물 세라믹 재료의 수중 레이저 빔 가공 시 가공 효율에 관한 연구가 제한적이다.

본 논문에서는 세라믹 화합물의 수중 레이저 빔 가공 시 가공 원리와 가공 특성에 대하여 연구하였다. 본 연구에서 실리콘 화합물의 수중 레이저 빔 가공은 다음과 같은 방법으로 가공 효율이 증대된다. 레이저 빔 조사로 인해 고온의 실리콘 화합물의 열수 부식 반응한다. 실리콘 화합물의 열수 부식 반응으로 인해 가공부의 산화물 형성이 차단되고 레이저 빔 가공의 효율이 향상된다. 또한 본 연구에서는 실리콘 화합물의 수중 레이저 빔 가공 시 가공 인자들의 영향에 대한 연구가 수행되었다. 물의 유속, 레이저 출력, 레이저 조사 횟수에 대한 파라미터 테스트가 수행되었으며, 그 결과 물의 유속이 증가할수록 좁고 깊은 채널 가공이 가능한 것을 확인하였다. 또한 같은 레이저 조건에서 물 속에서 가공 시 공기

중 보다 더 깊은 채널 가공이 가능한 것을 확인하였다. 마지막으로 본 연구에서 제안하는 수열 반응 레이저 빔 가공을 이용하여 실리콘 화합물 재료에 다양한 마이크로 형상을 제작하였다. 마이크로 채널 배열, 마이크로 핀 배열, 마이크로 절단 가공을 통해 실리콘 화합물 재료에 다양한 마이크로 구조물 제작이 가능한 것을 확인하였다.

**주요어:** 수중 레이저 빔 가공; 실리콘 화합물 세라믹; 질화 규소; 탄화 규소; 열수 부식; 마이크로 스트럭처링

**학번:** 2014-21837